1971

The effect of cathodic protection on the stress corrosion characteristics of 300M low alloy steel

John Pechonick

THE EFFECT OF CATHODIC PROTECTION ON THE STRESS CORROSION CHARACTERISTICS OF 300M LOW ALLOY STEEL

BY

JOHN PECHONICK, 1943-

A THESIS

Presented to the Faculty of the Graduate School of the

UNIVERSITY OF MISSOURI-ROLLA

In Partial Fulfillment of the Requirements for the Degree

MASTER OF SCIENCE IN METALLURGICAL ENGINEERING

1971

Approved by

Carlo Lorenzino (Advisor) Fred Kisslinger

Edward P. Hamsey

ABSTRACT

The objective of this investigation was to determine if stress corrosion failure of 300M steel is accelerated by the application of cathodic protection. Testing was conducted on notch tensile specimens that were coated with vacuum cadmium, electroplated cadmium, and vacuum aluminum. All specimens were stressed and placed in an aqueous sodium chloride environment. The failure times for the specimens were monitored and graphs were drawn which characterized the stress corrosion resistance of 300M steel and the cathodic protection systems. Fractography techniques were used to study the failure surfaces to determine the type of failure mechanism.

The results of this thesis program indicated that, for 300M low alloy steel:

1) The hydrogen evolved during cathodic protection of 300M steel by vacuum aluminum and vacuum cadmium embrittles the steel and accelerates failure.

2) Cathodic protection afforded by vacuum cadmium accelerates stress corrosion failure of 300M steel at all stress levels and significantly below 60% NTS.

3) Vacuum aluminum does not afford adequate protection to 300M steel and premature failure can be expected at all stress levels.

4) Electroplated cadmium affords excellent cathodic

protection to 300M steel and does not accelerate failure.

5) A notch through the cathodic coating to the base steel does not increase the failure susceptibility of 300M steel.

PREFACE

The author wishes to thank McDonnell Douglas Corporation for the use of their equipment, facilities, and library during this test program. Also, the author wishes to thank the following people for their valuable assistance during this test program: E. R. Fannin for his assistance in selecting a subject and machining the specimens, J. Holmes for his help in plating the test specimens, H. M. Keeser for his help in obtaining the necessary test equipment, B. Wilcox for his help in preparing the metallographic specimens and taking the electron microscope pictures, and to his thesis advisor, Carlo B. Sonnino, Professor of Metallurgy, St. Louis Graduate Engineering Center, University of Missouri - Rolla, for his technical assistance during the development of this thesis program.

TABLE OF CONTENTS

LIST OF ILLUSTRATIONS

LIST OF TABLES

I. INTRODUCTION

A. Statement of Problem

Aerospace and hydrospace designers make extensive use of low alloy high strength martensitic steels in structural applications. While these martensitic steels offer the designer excellent strength-to-weight ratio, they are very susceptible to corrosion when exposed to environments of temperature change, moisture, and salt air. The standard procedure for improving the corrosion resistance of these steels is to electroplate or vapor deposit with an anodic metal. If the plated coating and the base metal are notched during service, a stress concentration develops which is susceptible to galvanic corrosion. The hydrogen liberated during corrosion at the base metal may embrittle the base steel and lead to accelerated stress corrosion. This failure mechanism has been termed hydrogen stress corrosion (1,2,3,). This mechanism has been reported as the cause of premature failures where steel was plated with a sacrificical cathodic metal, like cadmium. It has been theorized that a notch, as described above, would greatly accelerate failure by hydrogen stress corrosion (1,4,5), but no data exists to comfirm this theory. The purpose of this thesis program is to determine if a notch exposing the base metal will, indeed, accelerate failure of cathodically protected

low alloy high strength martensitic steel.

B. Reason For Selection

The need for higher and higher strength steels is continually increasing with the design of advanced structures for hostile environments. This has resulted in demands for protective coatings that do not impair the mechanical properties of the coated metals. Before attemping to design these structures for minimum weight, it must be determined if premature failure is accelerated by cathodic protection. If cathodic protection does accelerate failure, the design limitations of low alloy steel cathodically protected must be defined and coatings recommended that do not limit their design usefulness.

Susceptibility of 300M low alloy martensitic steel to premature failure will be evaluated by subjecting bare and cathodically protected steel specimens to sustained load testing in an aqueous sodium chloride environment. Curves will be plotted that characterize the effects of various cathodic metals on the sustained load characteristics of 300M. These curves will plot time to failure versus load and will be used to determine if the various coating accelerates or inhibits premature failures.

The scanning electron microscope and macro-camera will be utilized to study the fracture surfaces and to determine the mode and type of failure. Previous investigators (6,7) have successfully used the above approach to study hydrogen embrittlement.

II. HISTORICAL BACKGROUND

The disastrous failures that can occur when static stresses are applied to metals in a corrosive enviroment have been thoroughly studied for centuries. But, the severe effect of hydrogen embrittlement on the mechanical properties and service life of high strength steels were not recognized until early days of World War II (8). The cause of a number of service failures was traced to the presence of hydrogen in the metal's lattice. Further investigation yielded the fact that electroplating or other cathodic processes were the mechanism by which the hydrogen entered the lattice of the steel.

During the late 1940's and early 1950's extensive studies were conducted to isolate and define the variables that cause hydrogen embrittlement of high strength steels. The results of these studies were that stress corrosion and hydrogen embrittlement are related and that it is impossible to separate the two mechanism. During corrosion it was theorized that hydrogen was liberated at the cathode. This liberated hydrogen diffuses into the corroding metal's lattice causing hydrogen embrittlement and accelerated failure by stress corrosion. Conversely, when a metal is charged with hydrogen by a cathodic process and a sustained load is applied a premature failure can occur which results from the lattice strain of hydrogen and the

inherent corrosion of the environment.

There are suprisingly few published papers dealing with the effects of cathodic protection interacting with stress and hydrogen embrittlement. Although authors have proved the three to be theoretically inseparable, the task of this program will be to determine if design allowances should be made in critical structural applications.

III. LITERATURE SURVEY

A. Mechanism of Hydrogen Embrittlement

There are no high strength steels which are immune to hydrogen embrittlement, but there are rather wide variations in the degree of susceptibility of the many types of steels. In general, these variations can be correlated with composition and microstructure of the steel. Embrittlement occurs at all stress levels, but it usually occurs in steels termed "ultra high strength", those above 200,000 psi stress level (9). In short term tensile tests, hydrogen embrittlement is manifested mainly as a loss of ductility. There is little or no influence on the yield point or the plastic properties up to the point where local necking occurs. The effect of hydrogen in steel is to prevent local necking from occuring as it does in steel free from hydrogen. Under the conditions of static loading in the presence of a notch, hydrogen causes premature failures at loads that may be as low as 20 percent of the normal ultimate tensile strength of the steel (10). The failure occurs by a process of crack initiation, growth, and overload.

The mechanism which precedes premature hydrogen embrittlement is the formation of an interstitial solid solution (4). Interstitial solid solutions are formed when solute atoms of small radii are accommodated in the interstices of the metal lattice. Because the size of the

lattice interstices is restrictive, only the smaller atoms like hydrogen, boron, carbon, nitrogen, and oxygen are likely to form this type of solid solution. Of these, the hydrogen atom with an atomic radius of 0.46 Å is the smallest, and hence, the most readily accommodated interstitially. When the lattice of a metal accepts a hydrogen atom, there is an accompaning expansion of the unit cell (4). Elsea and Fletcher (3) have observed bowing of thin sheets of steel after they were charged with hydrogen cathodically. The author has observed titanium failures during chemical milling. These failures were caused by high concentrations of hydrogen being induced into the titanium during chemical milling. When a stress concentration is present in a steel, the hydrogen that occludes in the unit cells near the concentration tends to expand the lattice near the tip of the crack and accelerates crack propagation until failure.

Conjecture exists as to the real mechanism of hydrogen embrittlement, but two prominent theories exist - the planar pressure theory and the hydrogen crack initiation theory. Zapffe and Sims (11,12) proposed that hydrogen embrittlement is a phenomenon of occlusion of molecular hydrogen under high pressure in voids which are a fundamental part of the crystal structure of the metal. When the occlusion pressure exceeds the elastic strength of the metal, slip and cleavage occurs much as during cold work. Thus, hydrogen embrittlement becomes nothing more than a phenom-

enon of internal precipitation of hydrogen along imperfectly disposed crystallographic planes. Troiano and his co-workers proposed a theory of hydrogen embrittlement (13) that relied upon the ability of hydrogen, the smallest interstitial solute element, to initiate cracks. According to their model, hydrogen migrates under the driving force of a stress gradient to a region where a triaxial stress condition exists. Here, the hydrogen reduces the "true cohesive strength" of the metal near the tip of a small void or crack. For the crack to propagate, hydrogen must diffuse to the new region of triaxiality near the base of the newly extended portion of the crack. The basic difference between the two theories is that the crack initiation model depends upon a series of incubations and crack extensions rather than a continuous process as proposed by the planar pressure.

B. Mechanism of Stress Corrosion

Stress corrosion of high strength steels often results in rapid premature failure. Stress corrosion is caused by low tensile stresses on a metal in a corrosive environment. Thus, it imposes severe limitations on the usefulness of any susceptible metal. Orginally, stress corrosion was considered to be simply a special case of electrochemical corrosion as described by Dix and his associates (14). This theory assumes that a crack propagates by continuous metal dissolution along an advancing front of corrosion. Later, a new theory

suggested by Keating (15) was based on a cyclic chemical mechanical mechanism. This theory assumes microscopic bursts of mechanical fracture alternating with short periods of corrosion. The following discussion will expand on the details of these two theories.

Dix and his associates (16) demonstrated the basic electrochemical nature of stress corrosion and the contribution of the mechanical mechanism to total failure. If corrosive attack penetrates preferentially along a narrow path a component of tensile stress normal to the path of corrosion creates a stress concentration at the base of the localized corrosion path. The deeper the corrosion and the smaller the radius at the base of the corrosion path, the greater the stress concentration. At sufficiently high stress concentrations, the metal pulls apart along these continuous localized paths by mechanical action. This picture of stress corrosion has not changed significantly, but it has been expanded on by Keating (15) and by Gilbert and Hadden (17). The extension of Dix theory is that the mechanical extension of the corrosion path exposes clean metallic surfaces, and the corrosive agent is immediately drawn into the crack by capillary action. This is followed by a period of rapid corrosion when the crack penetrates deeper in the metal. Also, there is an accompaning lateral corrosion action which results in branching of the corrosion path at each

arrest. It seems reasonable that the major factor in penetration of a crack is the result of mechanical action rather than electrochemical action. Thus, the above discussion depicts essentially two stages, a period of localized electrochemical corrosion, followed by a mechanical stress cracking stage.

While the mechanisms which have been discussed above have many attractive features, the importance of environment and alloy composition are not fully explained. A service environment which is rich in hydrogen may accelerate crack extension and cause premature failure (18).

C. Interaction of Hydrogen Embrittlement and Stress Corrosion

It is common practice to apply cathodic protection to steel parts that are exposed to corrosive environments during service. The objective is to maintain strength of the steel by preventing corrosion which would reduce the effective cross-sectional area and the load carrying ability. In any cathodic protection system that is commercially economical, the cathode potential will usually be such that some atomic hydrogen will be deposited on the surface of the steel (19). This applies to systems of imposed cathodic current as well as sacrifical cathodic protection. Although hydrogen is insoluble in steel at ambient temperatures and pressures, atomic hydrogen can readily enter steel and may attain a concentration

as high as 12-14 ppm (19).

McEowen and his co-workers (19) studied the effects of cathodic protection on high strength steels and found that the steel absorbs hydrogen while under a sustained tensile stress. The results of these studies showed that fracture occurs in a brittle manner which is typical of hydrogen embrittlement.

Copson (2) in his classification of stress corrosion cracking failures indicates that hydrogen can be generated by cathodic protection and results in accelerated stress corrosion failure.

A personal contact was made by the author to Mr. A. R. Elsea, Battelle Memorial Institute, to discuss the effects of cathodic protection on stress corrosion (20). Mr. Elsea indicated that sacrifical cathodic protection accelerates stress corrosion failure. He stated that his most recent work was done under contract and was considered proprietary.

Barnartt (21) states that cathodic current will arrest stress corrosion and in some cases stop the penetration of cracks after they have initiated. In this case, he considers that the cathodic current imposed stops the corrosion process on the steel which is necessary for stress corrosion. Sonnino and his co-workers, (22) while working with 18% maraging steel, concluded that sulfide corrosion was caused by an electrochemical mechanism of stress corrosion. When anodic current was impressed, the cracking time was reduced while cathodic current increased failure time.

Few papers have been published on the relationship of hydrogen embrittlement and stress corrosion. This thesis program will take an unique engineering approach to the problem in hopes of better defining the effects of cathodic protection and stress corrosion of high strength steels.

D. Test Methods to Evaluate Stress Corrosion Susceptibility

The majority of the investigators who are presently studying stress corrosion and hydrogen embrittlement are using various types of sustained load tests. Some of the test methods being used are as follows: ring test (23), C-clamp test (24), beam test (25), bolt test (26), and the notch tensile test (27). All the above tests place the test specimen under a stress with a constant load. Ketcham, (28) who chairmaned the ASTM Task Group 1 on stress corrosion testing methods outlines the various methods listed above. All the various methods have their own inherent advantages. Geyer and his associates (27) concluded that the most sensitive method of evaluating stress corrosion and hydrogen embrittlement was the notch tensile test with a three thousandth notch root radius.

In any type of failure investigation, an important aspect of the analysis centers around locating the origin or nucleus of the fracture. The origin usually holds the key to the reason for failure. The ability to trace fracture propagation on test specimens depends on macroscopic fea-

tures such as chevron marks, localized zones of plane strain, hackle marks, beach marks, etc. (29). The electron microscope and optical macrocamera are the most helpful tools available to the failure analyst.

IV. TEST PROCEDURE

A. Test Material

The test material selected for this test program was 300M low alloy martensitic steel. This material was selected because it is utilized by designers where ultra high strength material in the 300 KSI stress range is desired. 300M per Aerospace Materials Specification 6417 is an ultra high strength low alloy martensitic steel which combines high hardenability with relatively good impact strength and ductility. It is primarily used in the form of bar, rod, tube, and forgings heat treated to 270 to 300 KSI stress level. A three-fourths inch diameter rod, fifty feet long, was purchased from Latrobe Steel Company for this test program. The composition of the rod was determined by atomic absorption spectrophotometry, and a comparison with the AMS specification is shown in Table I.

B. Specimen Fabrication

Tensile and sustained load specimens were fabricated as shown in Figure 1 and 2, respectively. The 3/4 inch diameter test material rod was rough turned on a lathe to 0.405 inch diameter and 103 three inch specimen blanks were sawed. These blanks were then center drilled and the neck section was turned to 0.275 inch diameter. The specimens

TABLE I

COMPOSITION OF TEST MATERIAL

Element	Weight Percent		
	AMS6417 Specification		Test Material
	Min.	Max.	Actual
Carbon	0.40	0.45	0.43
Manganese	0.65	0.90	0.69
Silicon	1.45	1.80	1.72
Phosphorous	-	0.03	0.01
Sulfur	-	0.03	0.01
Chromium	0.65	0.90	0.74
Nickel	1.65	2.00	1.80
Molybdenum	0.30	0.45	0.39
Vanadium	0.05	-	0.07
Iron	Balance		Balance

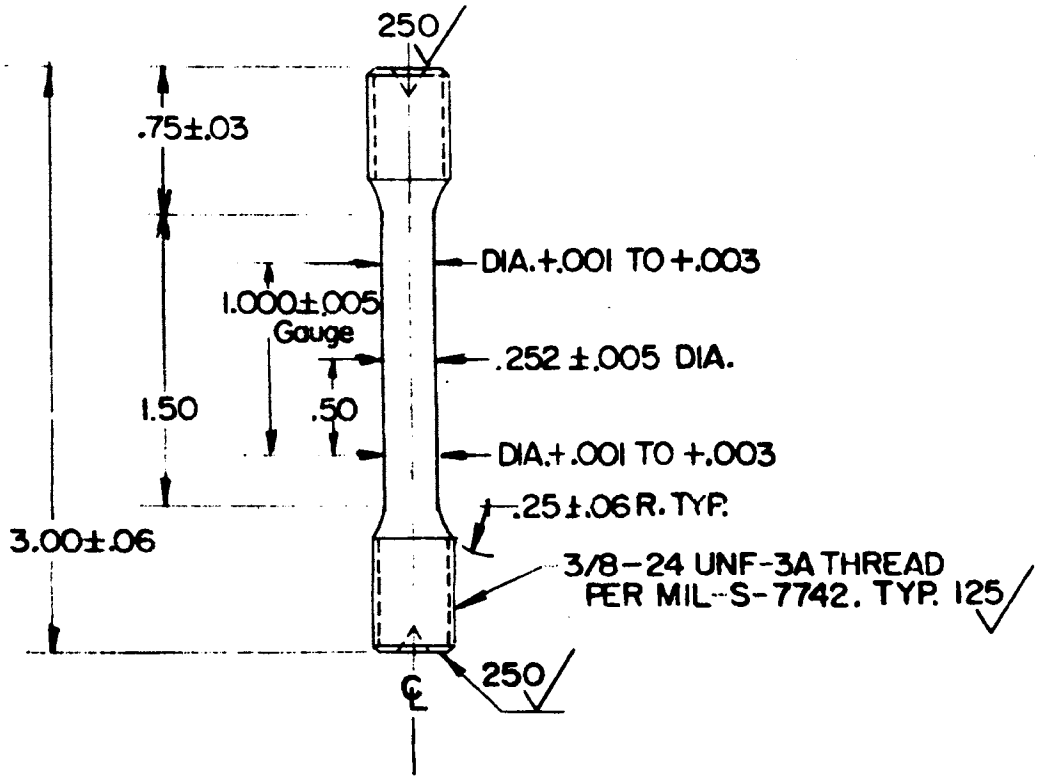

1. ALL REQUIRED HEAT TREATMENT SHALL BE PERFORMED PRIOR TO FINISH MACHINING.
2. DO NOT GRIND.
3. SPECIMEN SHALL BE CONCENTRIC WITH THREADS WITHIN .005 FIR.
4. CENTER OF GAUGE MUST BE SMALLER THAN ENDS WITHIN THE SPECIFIED TOLERANCE. TAPER MUST BE GRADUAL.
5. SURFACE ROUGHNESS PER MIL-STD-10. 63 RHR EXCEPT AS NOTED.
6. SPECIMEN SHALL BE FREE OF NICKS, DENTS, SCRATCHES AND MACHINING MISMATCH.

FIGURE 1

CONFIGURATION OF TENSILE SPECIMEN

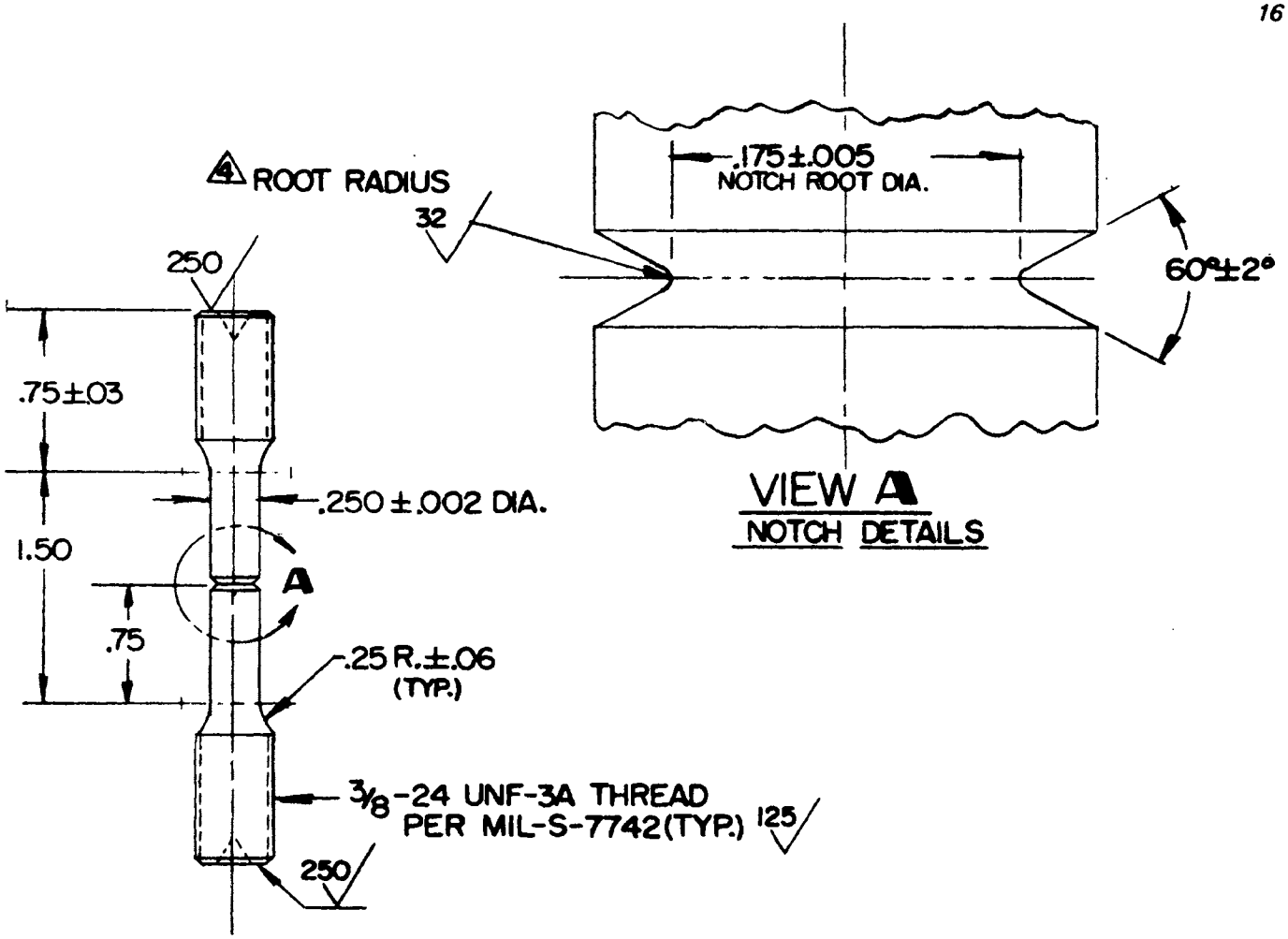

1. ALL REQUIRED HEAT TREATMENT SHALL BE PERFORMED PRIOR TO FINISH MACHINING.
2. DO NOT GRIND.
3. CONCENTRICITY OF NOTCH AND THREADS, .001 FIR.
   CONCENTRICITY OF NOTCH AND REDUCED DIA. SECTION, .002 FIR.
4. NOTCH ROOT RADIUS SHALL BE 0.003 INCH.
5. SURFACE ROUGHNESS PER MIL-STD-10. 125 RHR EXCEPT AS NOTED.
6. SPECIMEN SHALL BE FREE OF NICKS, DENTS, SCRATCHES AND MACHINING MISMATCH.

FIGURE 2

CONFIGURATION OF SUSTAINED LOAD SPECIMEN

were heat treated according to the schedule in Figure 3. After heat treatment, the specimens were finish machined by grinding the neck section to 0.250 inch diameter and the thread ends to 0.375 inch diameter. The notches were then machined to a 0.003 inch radius by grinding and the threads were made using a single point tool. All specimens were inspected to determine the root radius, notch diameter, and eccentricity of the notch diameter and specimen neck diameter. Appendix 1 contains the inspection records for all specimens used in this thesis program.

C. Test Equipment

Sixteen test cells were fabricated from 2024-T4 aluminum, see Figure 4. Aluminum plate was sawed into four by four by two and one-half inch squares, and a three inch diameter hole was bored through the center of the squares. One inch diameter fixture holes were match drilled on the top and bottom of the squares. Also, a one-fourth inch diameter half alignment hole was drilled on the circumference of the fixture hole. The test cell was then hard anodized to provide abrasion and corrosion resistance. To apply the load to the specimens, one inch diameter 4340 AISI steel pins were used, see Figure 5. The pins were threaded on one end and the opposite end was drilled and tapped to fit the threads on the test specimen. One-fourth inch diameter

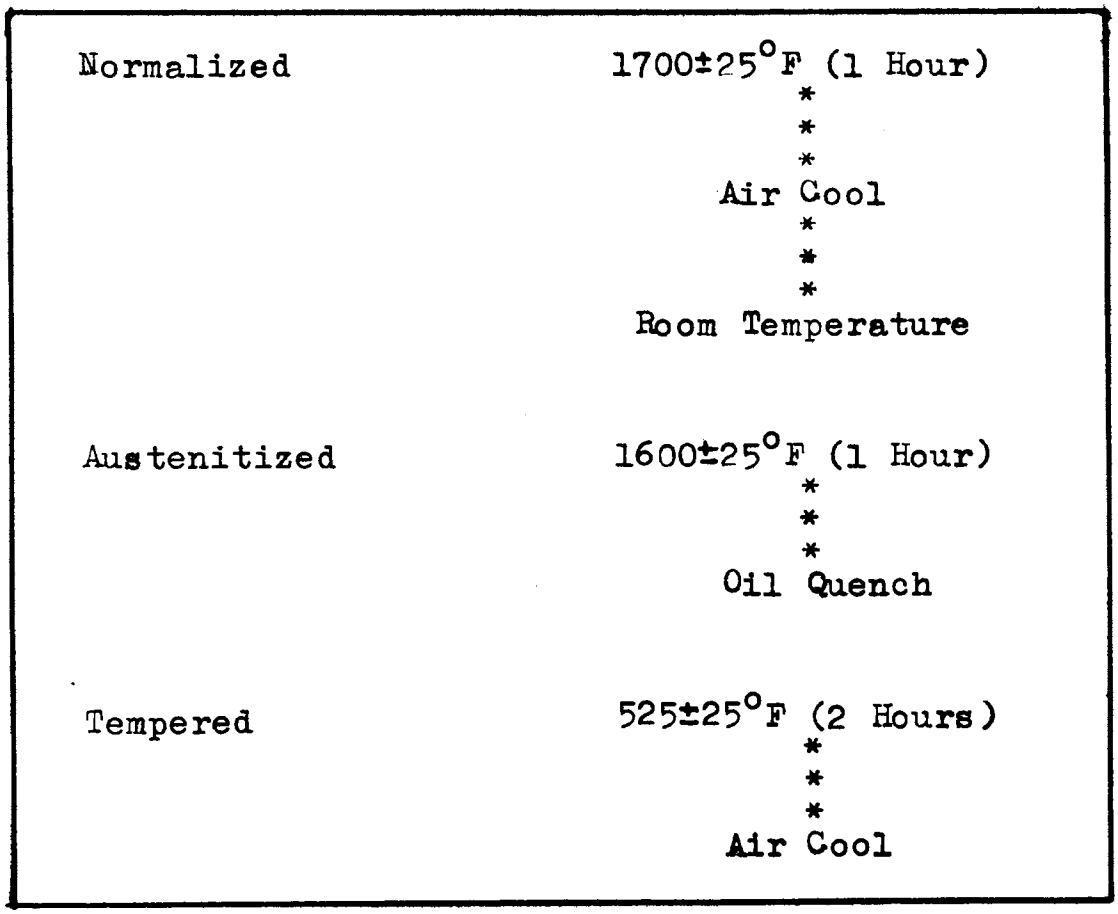

FIGURE 3

HEAT TREATMENT SCHEDULE

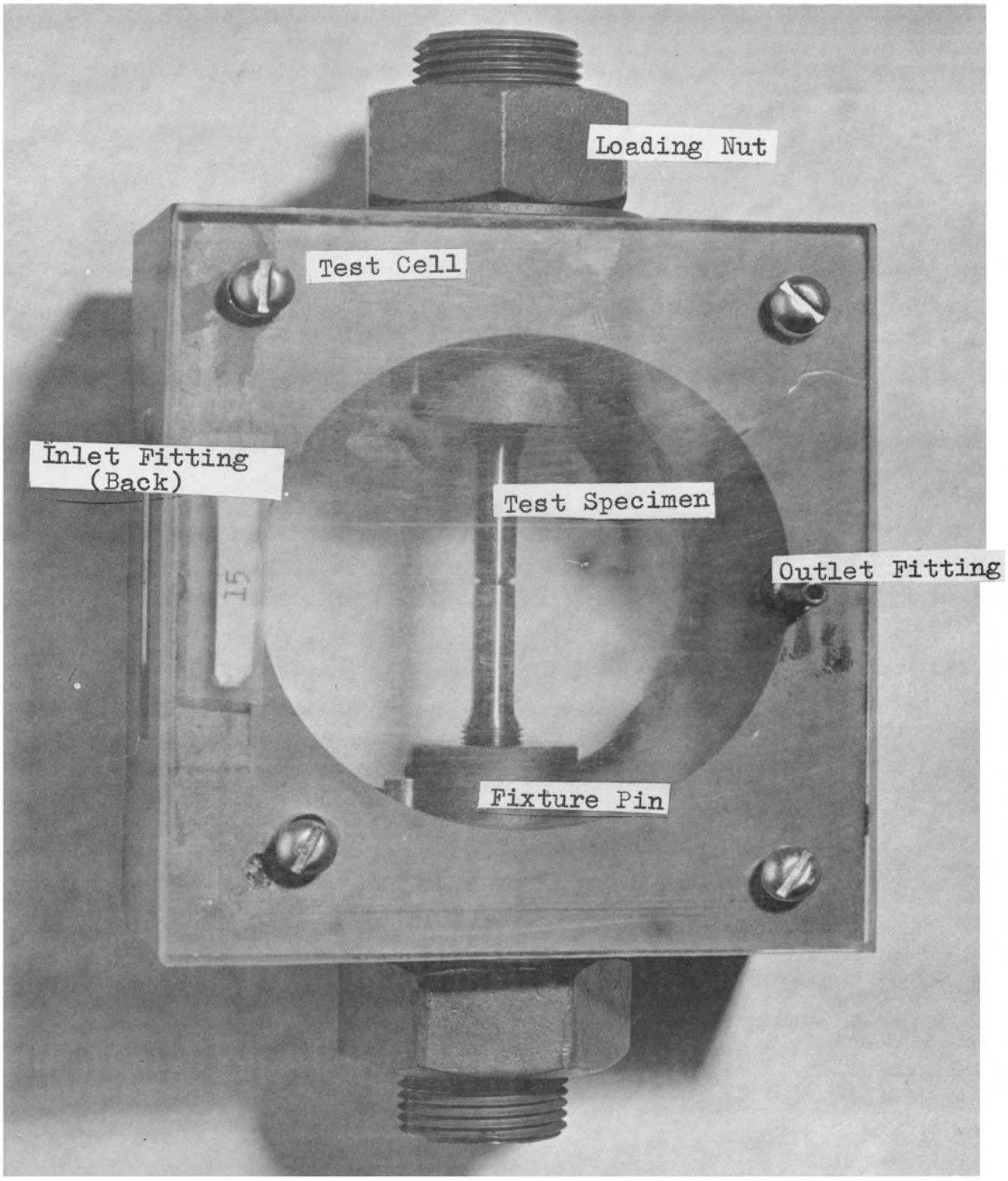

FIGURE 4

PHOTOGRAPH OF ASSEMBLED TEST CELL

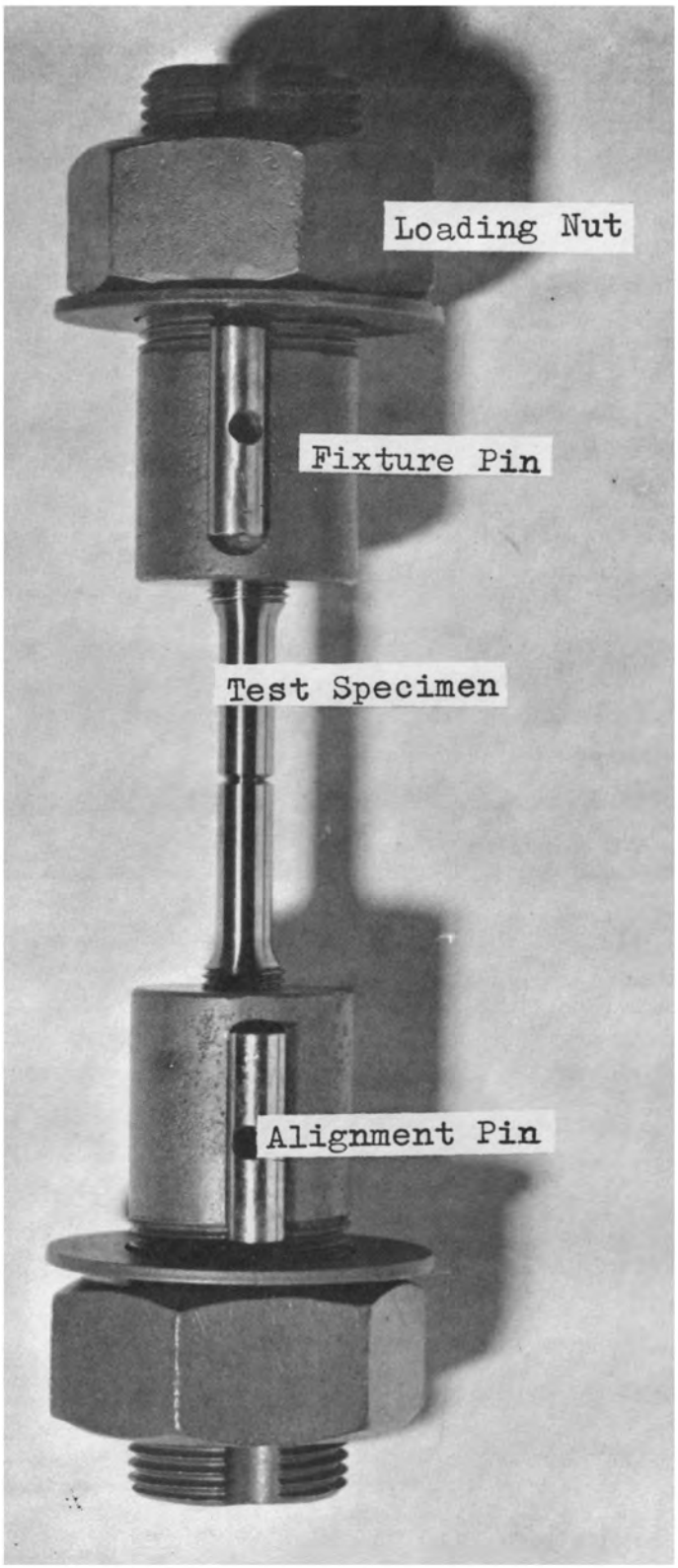

FIGURE 5

PHOTOGRAPH OF TEST SPECIMEN AND STRESSING FIXTURE

stainless steel pins were used for aligning the specimen fixture and the test cell. A Plexiglass plate was cemented to the back of the test cell. Holes were drilled and tapped in the front side of the test cell to facilitate fastening Plexiglass plates. Liquid inlet and outlet fittings were cemented on the front-bottom and back-top of the cells.

The sixteen test cells were ganged together with plastic tubing and copper tees to a liquid inlet manifold and to a liquid outlet reservoir. The test solution was pumped from the liquid outlet reservoir to the liquid inlet manifold and flowed through the labyrinth of tubes and tees to the test cells. The pump was wired to a sequential timer which activated the pump for thirty seconds every fifteen minutes. This cycle caused the test cells to be filled with 3.5% aqueous NaCl electrolyte 50% of the test time. While the pump was not operating the electrolyte drained out of the cells and the cells were empty 50% of the test time.

D. Test Specimen Loading

A unique method was devised for loading the test specimens. Specimen No. 92 and 93 were used to establish a relationship between load and strain gauge reading. Strain gauges were placed 90 degrees from each other and three-eights inch from the notch. Strain gauge readings were tabulated versus applied load until the specimens failed. The applied load was divided by the cross sectional area of the test specimen at the base of

the notch. Appendix 2 contains the strain gauge readings as a function of actual applied load, stress at the base of the notch, and test loads designated as percent of the notch tensile strength (NTS). The notch tensile strength (NTS) of the test specimens was 399 KSI. Strain gauges were placed on specimens 4 - 91 precisely as they were placed on the calibrations specimens 92 and 93. The test specimens were loaded to the strain that corresponded to the percent of the notch tensile strength (NTS) desired.

E. Specimen Test Procedure

Table II outlines the test schedule for the specimens in this test program. Specimens 1-3 were tensile tested and specimens 4-91 were sustain load tested. Electroplated cadmium, vacuum deposited cadmium and aluminum were the cathodic coatings selected for evaluation. All "notched" specimens were completely coated in the notch area and one-quarter of an inch up the specimens in both directions. A 0.005 inch wire was wrapped around the base of the notch on all "notch exposed" specimens before the coating was applied. After coating the wire was removed and the base of the notch was uncoated or "exposed". The electroplated cadmium and vacuum cadmium were applied at McDonnell-Douglas, St. Louis, and the vacuum aluminum was applied by Anadite Corporation, Los Angles. Specimens were tested at each stress level in both the "notched" and "notch exposed" conditions. The test specimens were placed in the test cells, loaded to test load, and exposed to an intermittent 3.5% aqueous NaCl electrolyte for 200 hours or until failure.

TABLE II

TESTING SCHEDULE

Specimen Number	Coating	Condition	Type of Loading
1-3	none	none	tensile test
4-7	none (control)	notched	90% NTS
8-11			75% NTS
12-15			60% NTS
16-19			40% NTS
20-22	Cd (vacuum)	notched	90% NTS
23-25			75% NTS
26-28			60% NTS
29-31			40% NTS
32-34	Cd (vacuum)	notched (exposed)	90% NTS
35-37			75% NTS
38-40			60% NTS
41-43			40% NTS
44-46	Cd (electro)	notched	90% NTS
47-49			75% NTS
50-52			60% NTS
53-55			40% NTS
56-58	Cd (electro)	notched (exposed)	90% NTS
59-61			75% NTS
62-64			60% NTS
65-67			40% NTS
68-70	Al (vacuum)	notched	90% NTS
71-73			75% NTS
74-76			60% NTS
77-79			40% NTS
80-82	Al (vacuum)	notched	90% NTS
83-85			75% NTS
86-88			60% NTS
89-91			40% NTS
92-93	none	notched	tensile test

V. TEST RESULTS

A. Tensile Tests

Tensile tests were conducted at room temperature in a standard tensile machine. The results are shown in Table III. All specimens exhibited ultimate tensile strength greater than 300 KSI and yield strength greater than 250 KSI as anticipated by a 525°F temper for two hours. The ductility of the steel, as measured by reduction of area and elongation, was excellent for a steel of the 300 KSI ultimate strength level. The average elongation and reduction in area were 11% and 42.3%, respectively.

B. Sustained Load Tests

The results of the sustained load tests are presented in Table IV. Here, the time to failure for all test specimens is tabulated. Also, the average time to failure is listed for each test condition. Figures 6, 7, and 8 are graphs which characterize the failure times versus load for the control specimens and the particular coating.

Figure 6 compares the bare 300M control specimen with the vacuum cadmium specimens and the exposed notch vacuum cadmium specimens. All of these specimens exhibited similar failure curves between 90% NTS and 60% NTS. Therefore, it can be concluded that a similar type of failure mechanism is controlling the rate of failure. It would seem logical

TABLE III

MECHANICAL PROPERTIES OF TEST MATERIAL

Specimen Number	Yield Strength (KSI)	Ultimate Strength (KSI)	Elongation (%)	Area Reduction (%)
1	256.9	310.2	11.0	43.4
2	256.8	310.5	11.0	42.6
3	256.9	310.7	11.0	41.0
Ave.	256.9	310.5	11.0	42.3

TABLE IV

RESULTS OF SUSTAINED LOAD TESTS

Specimen No.	Specimen Coat./Cond.	Specimen Load (%NTS)	Failure Time (hrs.-mins.)	Average Failure Time (hrs.-mins.)
4	control (bare) notched	90	1-40	2-01
5			2-25	
6			0-50	
7			3-30	
8		75	3-30	4-15
9			5-05	
10			4-10	
11			21-15*	
12		60	7-05	7-51
13			10-00	
14			6-05	
15			8-15	
16		40	>200-00	>200-00
17			>200-00	
18			>200-00	
19			>200-00	
20	Cd (vacuum) notched	90	0-45	1-36
21			2-05	
22			2-50	
23		75	2-55	3-23
24			3-50	
25			65-00*	
26		60	5-05	6-45
27			8-40	
28			6-30	
29		40	18-30	23-45
30			29-00	
31			3-05*	
32	Cd (vacuum) notched (exposed)	90	2-00	2-20
33			3-10	
34			2-25	
35		75	2-40	4-48
36			6-30	
37			4-15	
38		60	5-30	8-02
39			8-20	
40			10-15	
41		40	15-20	26-20
42			30-15	
43			33-30	
44	Cd (electro)) notched	90	3-55	3-13
45			20-10*	
46			2-30	
47		75	4-10	5-20
48			6-30	
49			32-15*	
50		60	5-50	9-45
51			11-20	
52			12-10	

TABLE IV (CON'D)

RESULTS OF SUSTAINED LOAD TESTS

Specimen No.	Specimen Coat./Cond.	Specimen Load (%NTS)	Failure Time (hrs.-mins.)	Average Failure Time (hrs.-mins.)
53	Cd (electro) notched (exposed)	40	49-00*	>200-00
54			>200-00	
55			>200-00	
56		90	2-20	3-10
57			3-50	
58			2-20	
59		75	5-15	6-48
60			8-20	
61			15-15*	
62		60	15-20	11-20
63			10-15	
64			8-25	
65		40	38-50*	>200-00
66			>200-00	
67			>200-00	
68	Al (vacuum) notched	90	0-15	0-35
69			0-30	
70			1-00	
71		75	1-25	1-16
72			1-00	
73			1-25	
74		60	5-30	3-40
75			2-15	
76			3-20	
77		40	4-15	10-00
78			10-20	
79			15-30	
80	Al (vacuum) notched (exposed)	90	1-20	0-56
81			1-00	
82			0-30	
83		75	2-05	3-38
84			22-00*	
85			5-10	
86		60	8-15	7-12
87			1-20	
88			6-10	
89		40	6-25	13-12
90			16-20	
91			22-50	

Note: * Asterisks indicate specimens improperly loaded

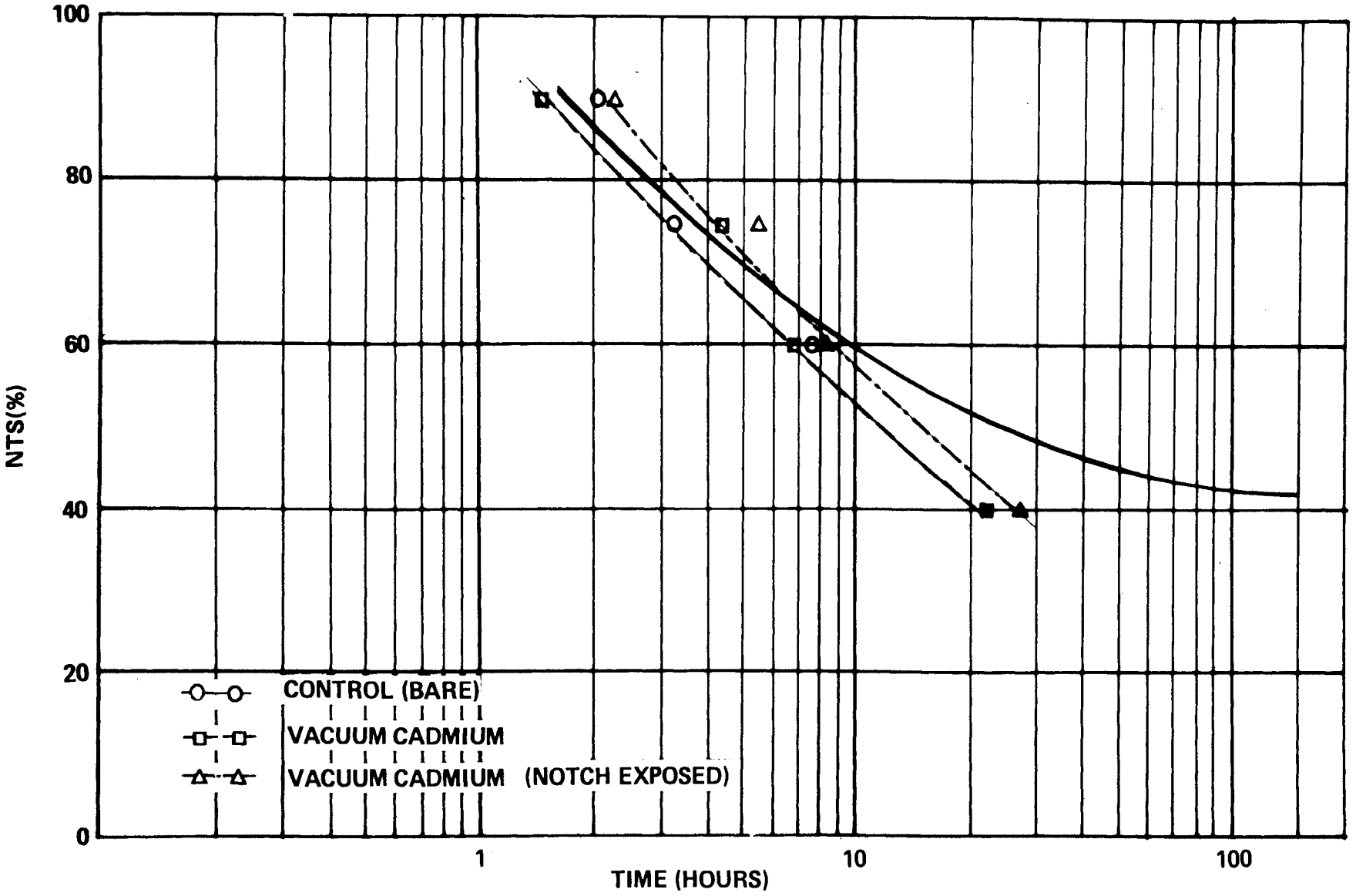

FIGURE 6

EFFECTS OF VACUUM CADMIUM ON STRESS CORROSION CHARACTERISTICS OF 300M

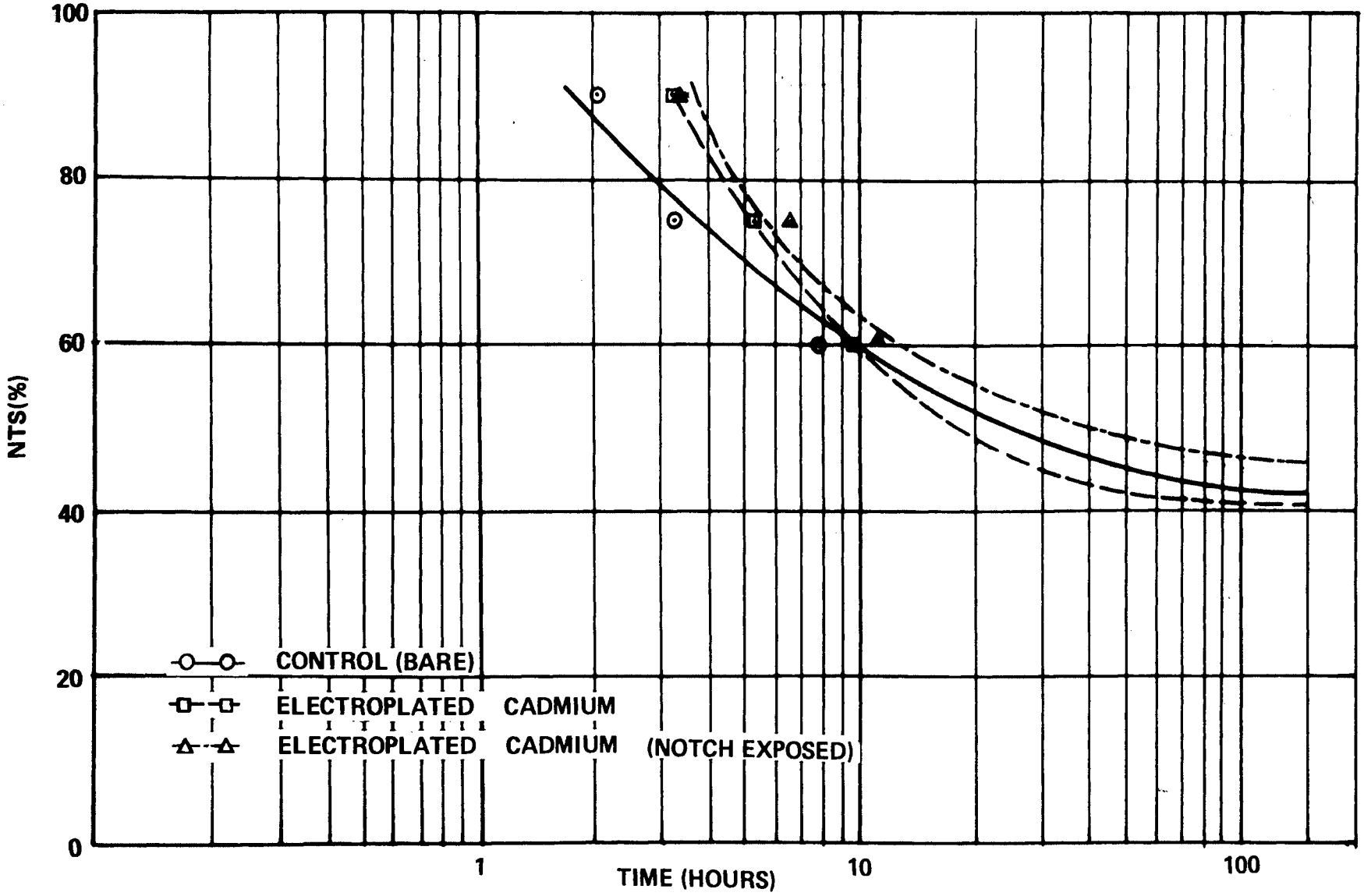

FIGURE 7

EFFECTS OF ELECTROPLATED CADMIUM ON STRESS CORROSION CHARACTERISTICS OF 300M

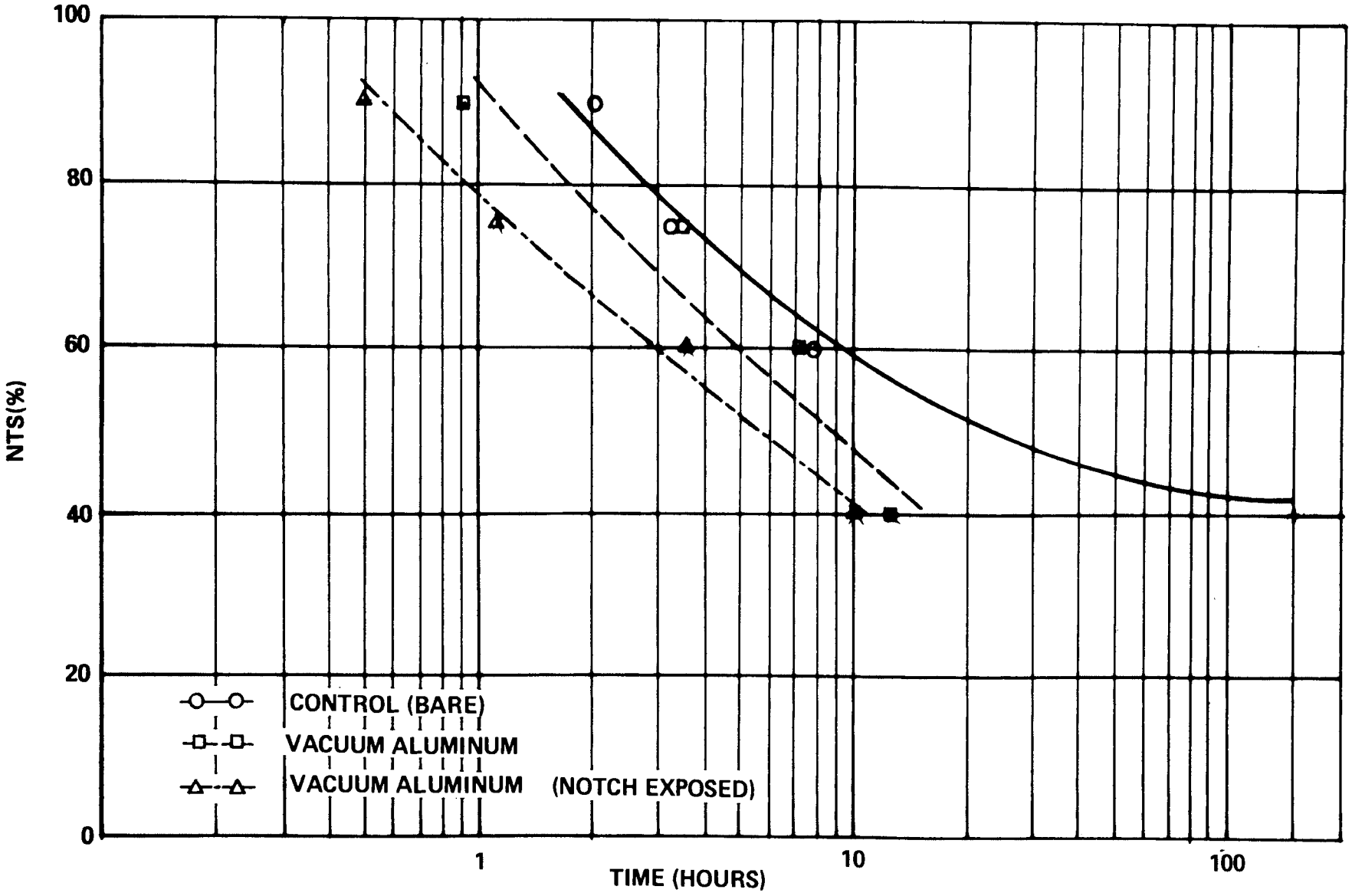

FIGURE 8

EFFECTS OF VACUUM ALUMINUM ON STRESS CORROSION CHARACTERISTICS OF 300M

that stress corrosion is controlling the failure and is overriding any effects of hydrogen embrittlement. This was concluded because the bare control specimens which were not subjected to any hydrogen enducing processes showed the same failure tendencies as the cadmium coated specimens. Below 60% NTS, the bare specimens became more resistant to failure than the cadmium coated specimens, and at 40% NTS the failure time of the bare specimens is greater than 200 hours. While the failure time for the notched and notch exposed cadmium coated specimens was less than thirty hours. It would be expected that the cadmium would offer protection to the steel and preclude premature failure. But, the accelerated failure indicates another mechanism must have control of the failure process. This mechanism is hydrogen embrittlement accelerated stress corrosion or hydrogen stress corrosion (1). The hydrogen liberated at the anodic steel during the corrosion of the cadmium embrittled the steel at the triaxial stress concentration near the notch and the specimen failed by a combination of the mechanisms.
If this were not the case, the cadmium coated specimens should have lasted as long or longer than the bare control specimens. The specimens with the notch exposed failed at approximately the same time as the specimens with notch that was not exposed. From these observations it can be concluded that the exposed notch does not accelerate failure. The failure mechanism is taking place on an atomic scale and the large size of the bare area, anode, does not concentrate the hydrogen in the

vicinity of the notch.

Figure 7 compares the bare control specimens with the electroplated cadmium notched and exposed notched specimens. In contrast to the curves for the vacuum coated specimens between 90% NTS and 60% NTS, the curves of the electroplated specimens differ somewhat from the curves of the control specimens. The electroplated specimens exhibited a longer sustained load life than the bare control specimens and when compared to the vacuum coated specimens the sustained load life is again much better. From this, it can be concluded that the electroplated cadmium affords better corrosion protection than does vacuum cadmium. The reason for the better corrosion protection is that the electroplated cadmium is more dense and has better base metal adhesion. Therefore, the electroplated cadmium acts as a better barrier against corrosion and prevents it from attacking the base metal. Below 60% NTS all three curves are similar, and the failure mechanism is stress corrosion. The good barrier presented by the electroplated cadmium prevents hydrogen embrittlement. Again, as with the vacuum coated specimens, the notch exposed specimen exhibited similar failure trends much the same as the specimens with the notch completely plated.

Figure 8 characterizes the effects of vacuum aluminum on the stress corrosion resistance of 300M steel. It is

quite evident from the graph that the aluminum reduces the failure time of the steel as compared to bare control and the cadmium coated specimens. Aluminum and cadmium occupy approximately the same relative position on the galvanic series with respect to steel; therefore, it would be expected that they would afford the steel equal cathodic protection and the failure times would be similar. This discrepancy can be explained by considering the surface activity of aluminum and cadmium in an aqueous environment. Aluminum has an inherent oxide film which is very obdurate and difficult to remove under ordinary atmospheric conditions. This film must be broken down before the aluminum can offer cathodic protection. While cadmium does not have a stubborn oxide film and can afford immediate and continuous cathodic protection. The graph shows a distinct difference between the specimens completely coated with aluminum and the specimens with the exposed notch. Because these curves are parallel with the control, it can be assumed that the failure mechanism is stress corrosion. The exposed notch concentrated the corrosion action in the area of maximum stress causing premature failure. Below 60% NTS both aluminum coated sets of specimens deviate from the control. A premature failure occurs that must be attributed to hydrogen embrittlement.

Asterisk in Table IV indicates specimens that deviate from the mean. This is attributed to poor strain gauge placement.

C. Sustained Load Test Specimens

Photographs of the test specimens after testing are shown in Figures 9 and 10. As is evident in the photographs, there is corrosion on all specimens after testing. This is evidence of stress corrosion and the possibility of accompaning hydrogen embrittlement. These photographs represent a typical specimen that failed at the 60% NTS stress level.

D. Scanning Electron Microscope Study

Failures caused by hydrogen embrittlement and stress corrosion are common in high strength steels, and it is very difficult to separate these two fracture types using standard electron fractography techniques. Figures 11 through 31 show photographs of a typical specimen that failed at 60% NTS. Each fractured specimen was examined by both optical and electron fractography. When examining the fracture surfaces, attention was given to the failure origin.

A binocular microscope was used to observe the fracture surfaces at low magnification. Figures 11, 14, 17, 20, 23, 26, and 29 show the fracture surfaces of typical test specimens. A rough textured slow growth area can be seen on all specimens where the fracture initiated, see arrows. This area is in contrast to the smooth textured overload failure area which is also quite evident.

Corrosion products are evident in Figures 11 and 23. These are not indicative of any failure mechanism and can be attributed to corrosion of the fracture surface after failure and prior to fractography study.

The key to determining the failure mechanism is locating the place where the fracture initiated. If the failure crack nucleates on the surface of the specimen, this is typical of stress corrosion. If the failure crack nucleates on the sub-surface of the specimen, this is typical of hydrogen embrittlement (31). The arrows on Figures 12, 15, 18, 21, 24, 27, and 30 indicate the orgin of the failure crack. In all cases it is apparent in the photographs that the failure initiated on the surface of the specimens. This would indicate a stress corrosion failure mechanism, but this can not be considered conclusive.

Figures 13, 16, 19, 22, 25, 28, and 31 are photographs of the slow growth fracture area and the overload failure area. The slow growth area is intergranular in nature with many secondary intergranular cracks. This is typical of both stress corrosion and hydrogen embrittlement failure mechanisms. There are no corrosion products evident in the intergranular area which would be expected with stress corrosion and not with hydrogen embrittlement type failures. The overload failure area is quite characteristic of a ductile failure. Micro dimples are shown in the photographs which are a result of the coalescing of

micro voids during the period when the load exceeds the ultimate tensile strength of the steel.

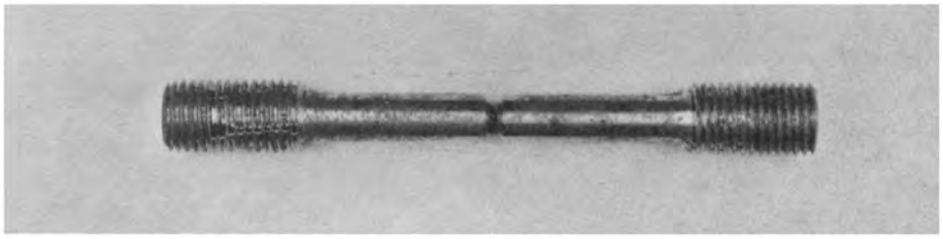

BARE CONTROL SPECIMEN

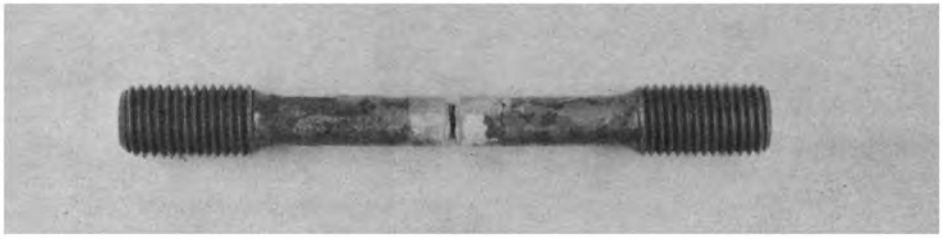

VACUUM CADMIUM SPECIMEN

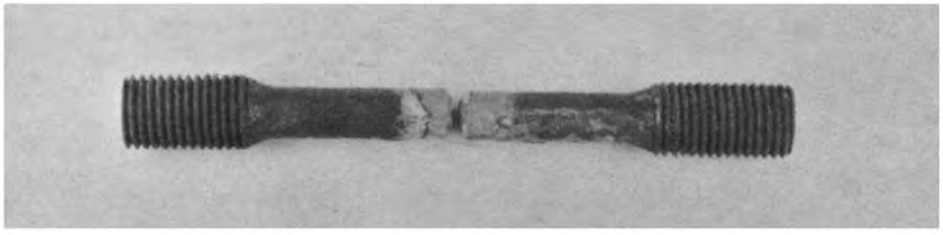

VACUUM CADMIUM (EXPOSED) SPECIMEN

FIGURE 9

PHOTOGRAPHS OF FAILED TEST SPECIMENS

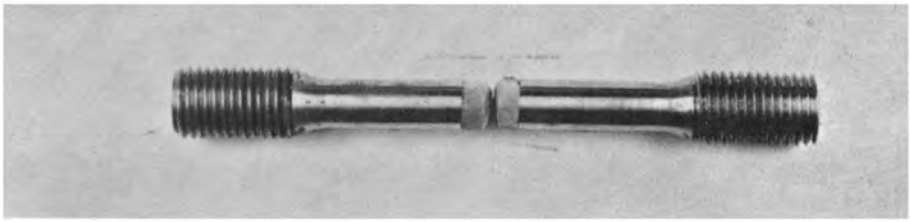

ELECTROPLATE CADMIUM SPECIMEN

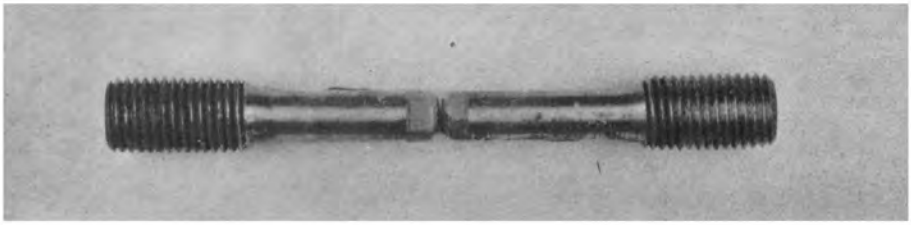

ELECTROPLATE CADMIUM (EXPOSED) SPECIMEN

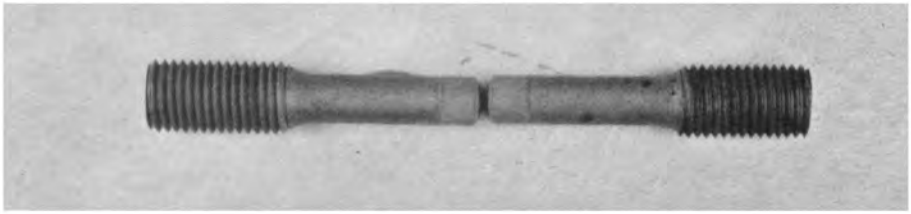

VACUUM ALUMINUM SPECIMEN

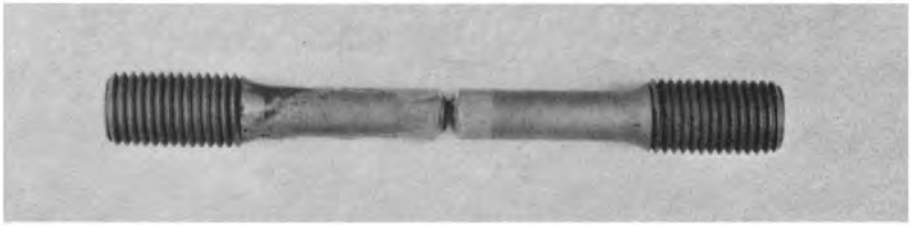

VACUUM ALUMINUM (EXPOSED) SPECIMEN

FIGURE 10

PHOTOGRAPHS OF FAILED TEST SPECIMENS

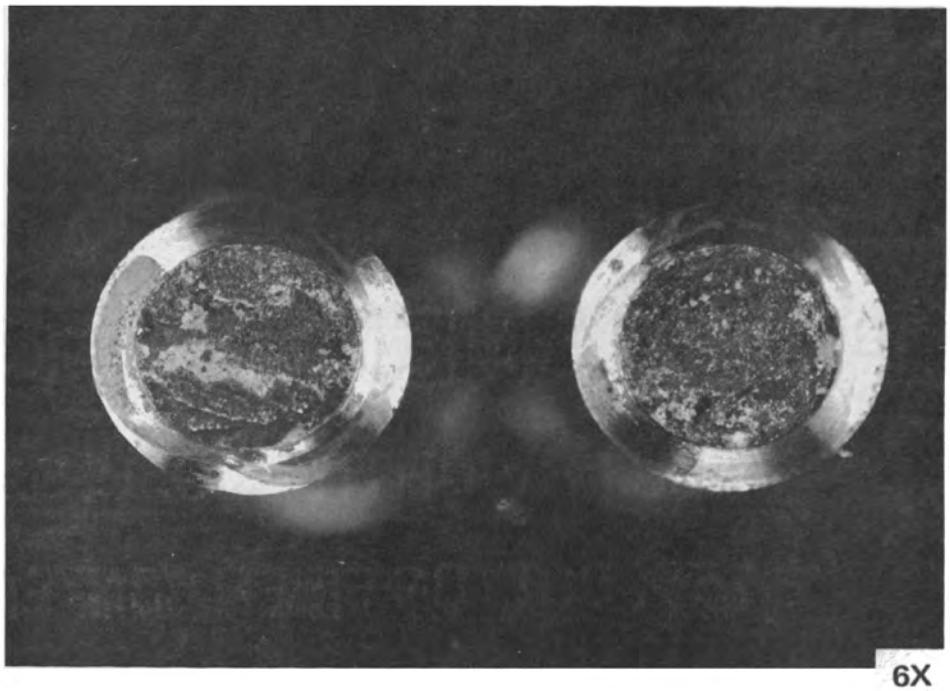

6X

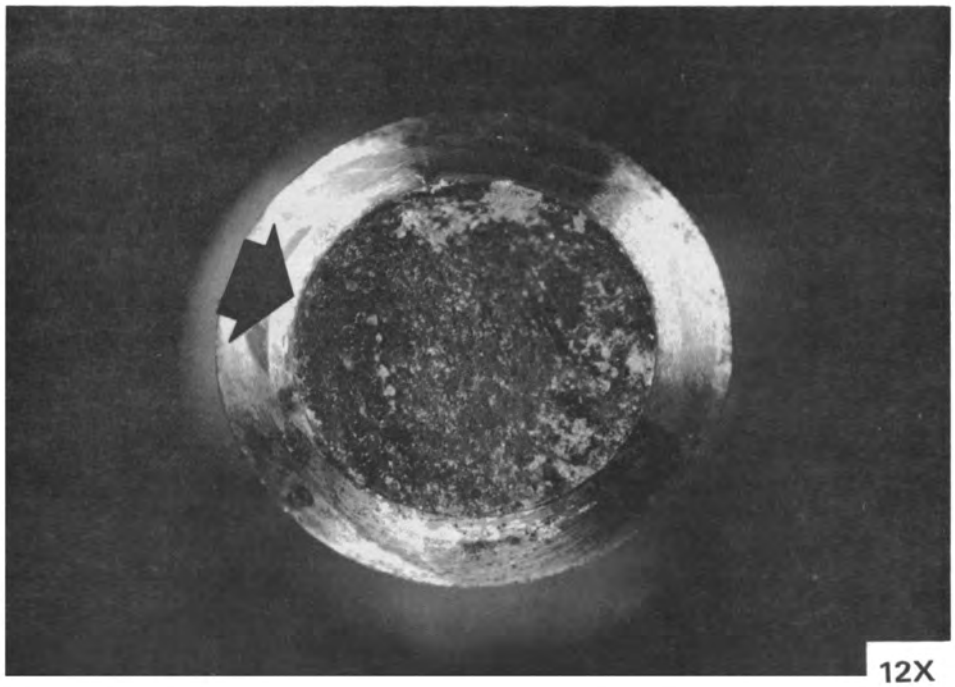

12X

FIGURE 11

MACROPHOTOGRAPHS OF CONTROL FRACTURE SURFACES

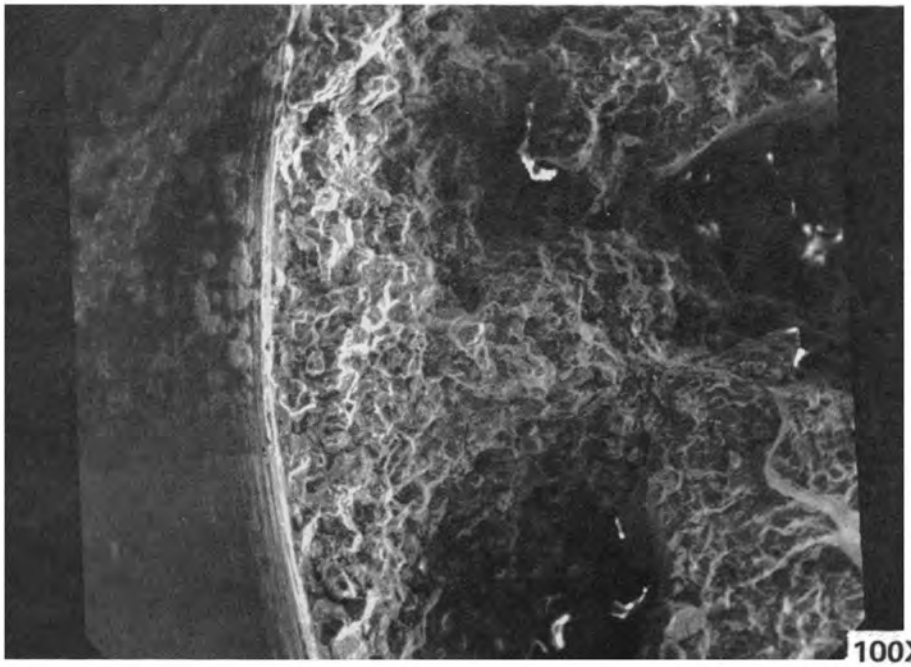

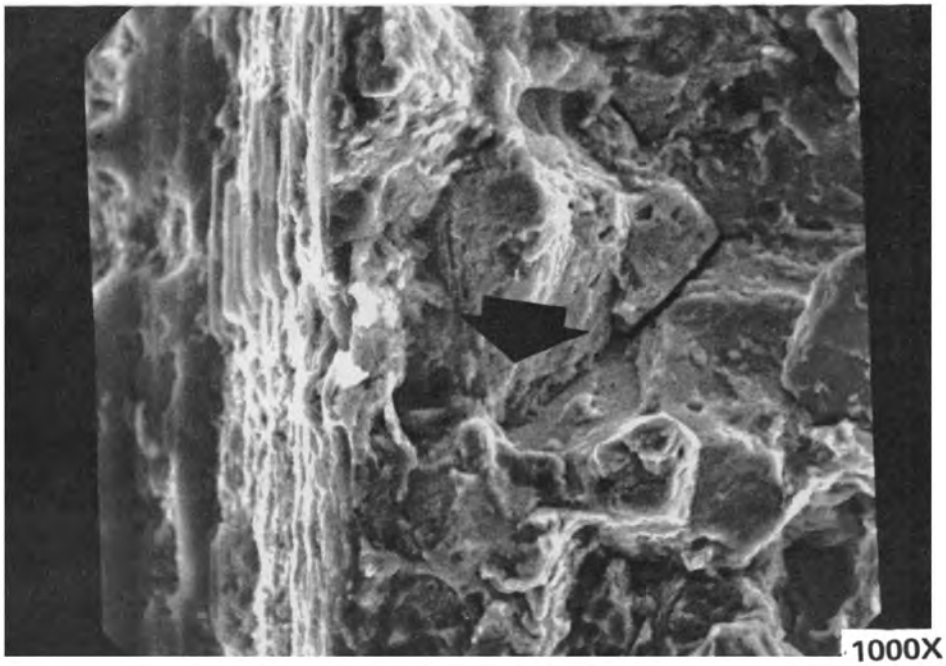

FIGURE 12

PHOTOGRAPHS OF CONTROL FRACTURE INITIATION

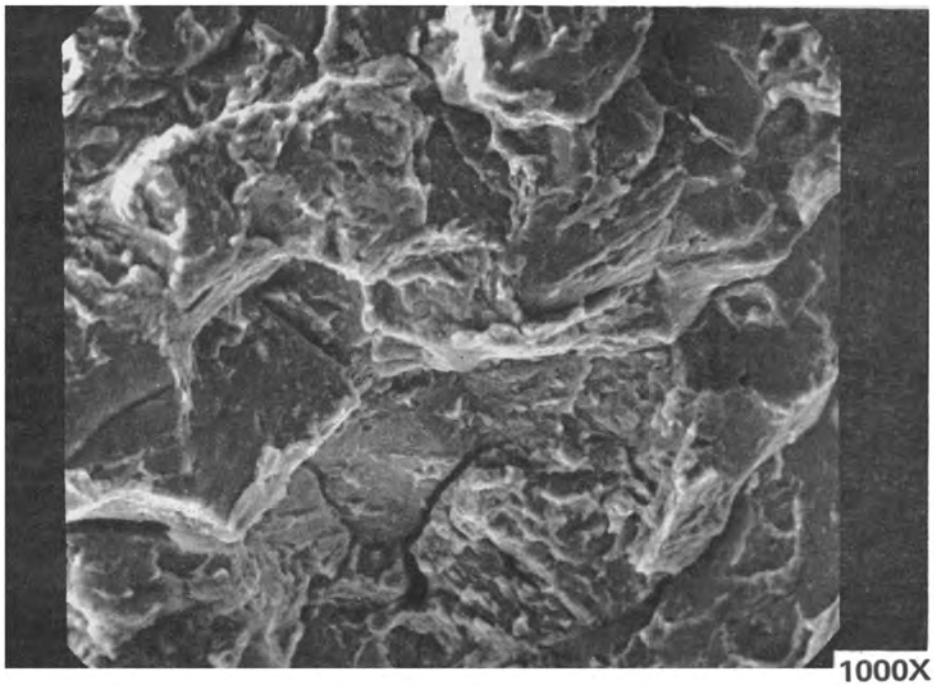

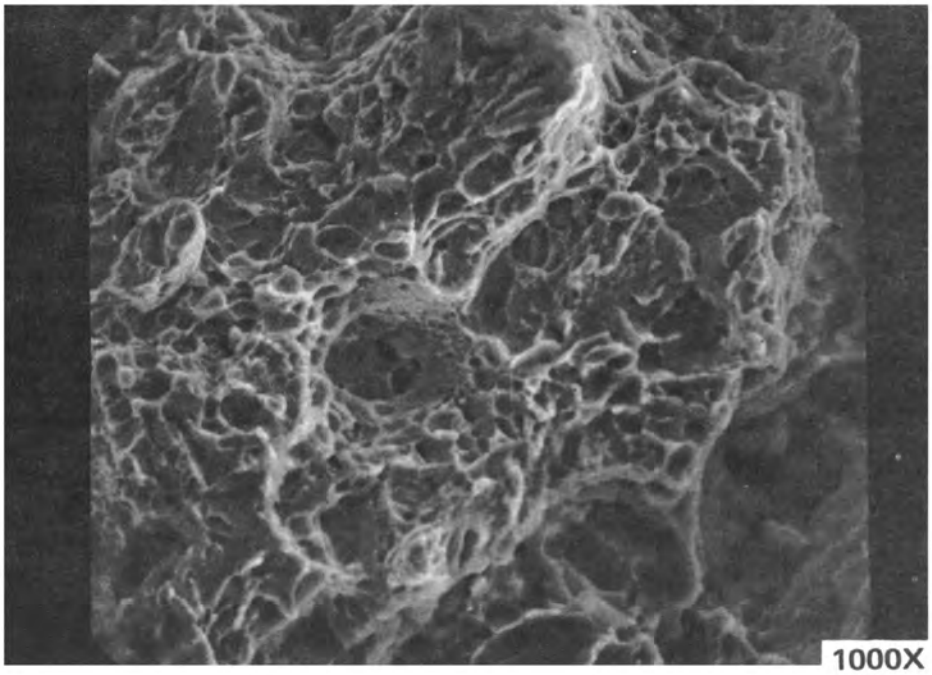

FIGURE 13

PHOTOGRAPHS OF CONTROL FRACTURE AREA

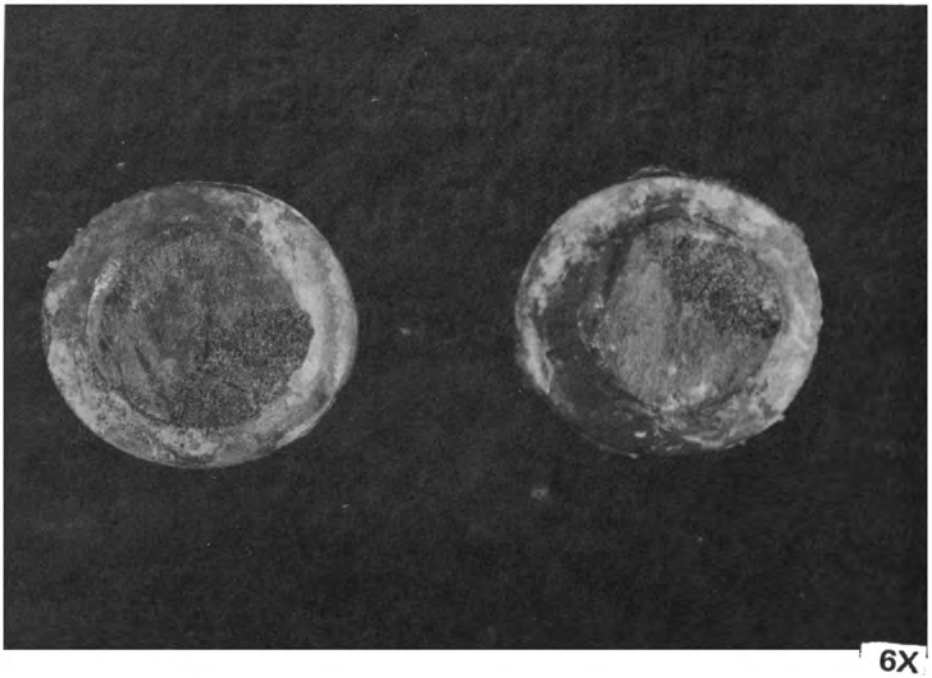

FIGURE 14

MACROPHOTOGRAPHS OF VACUUM CADMIUM FRACTURE SURFACES

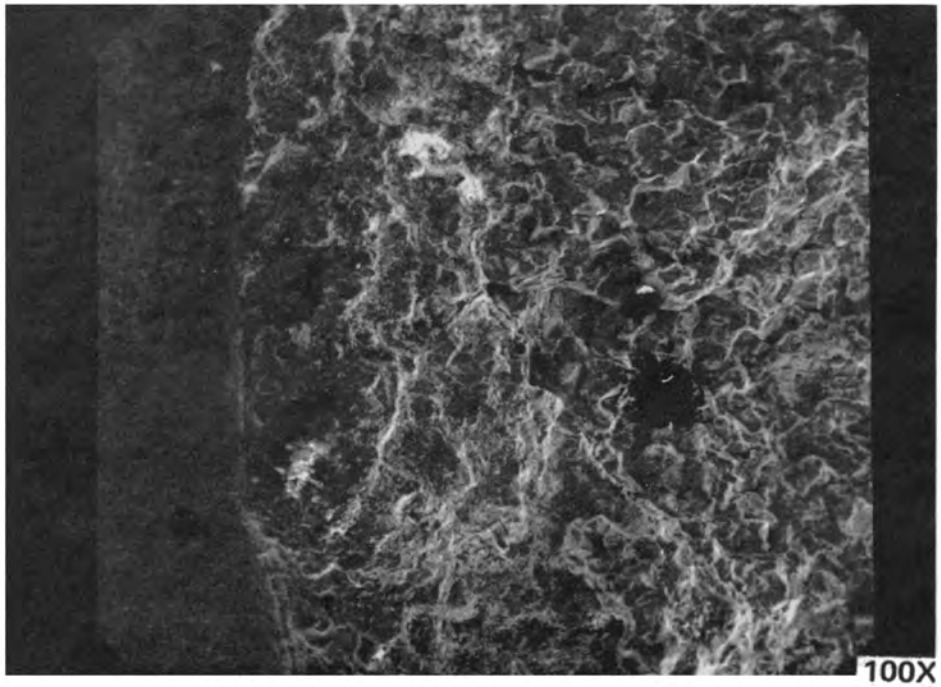

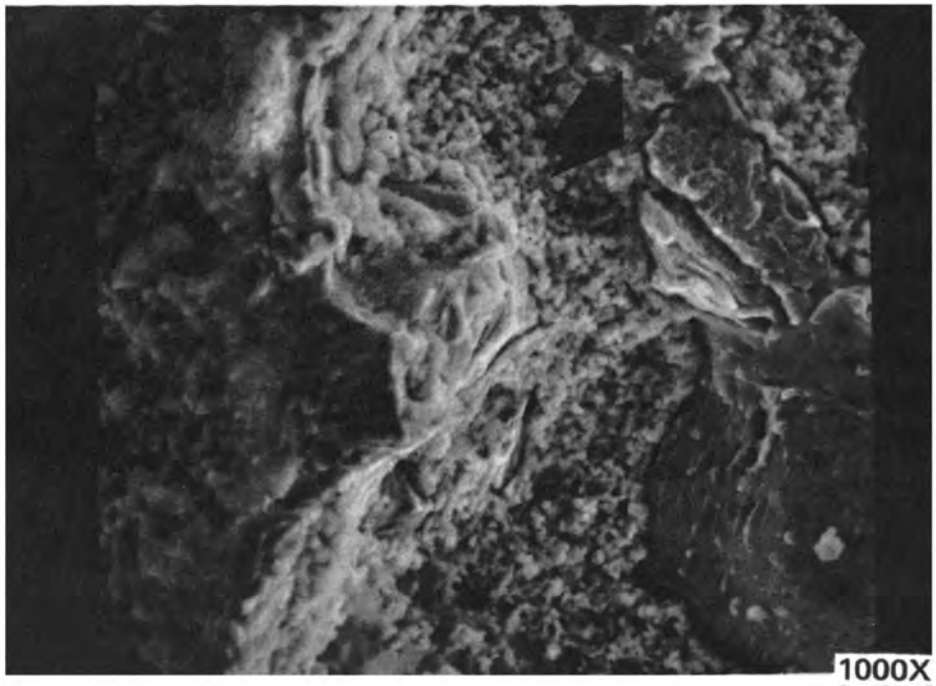

FIGURE 15

PHOTOGRAPHS OF VACUUM CADMIUM FRACTURE INITIATION

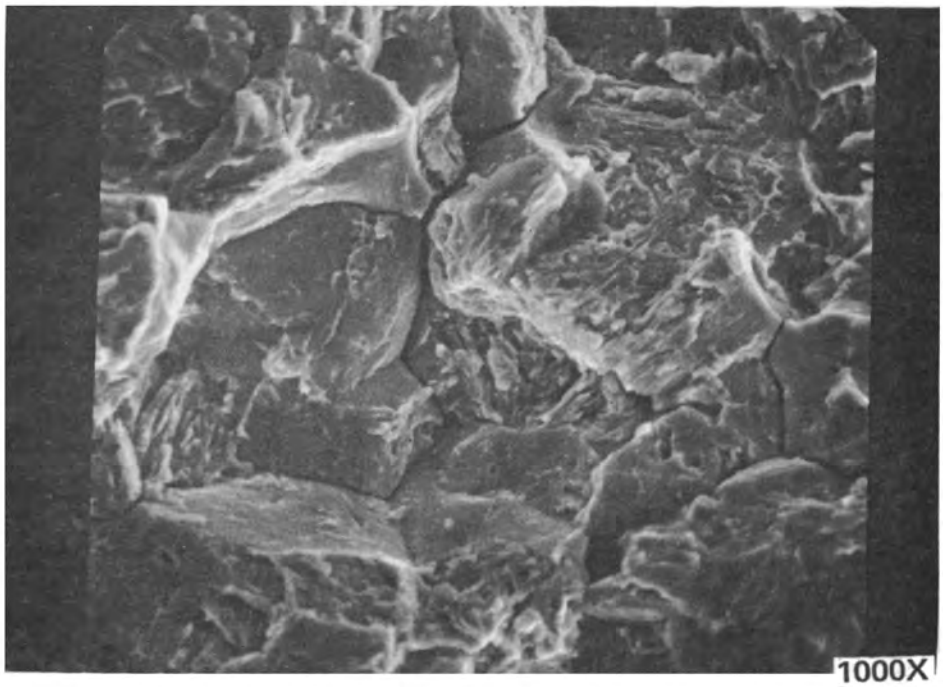

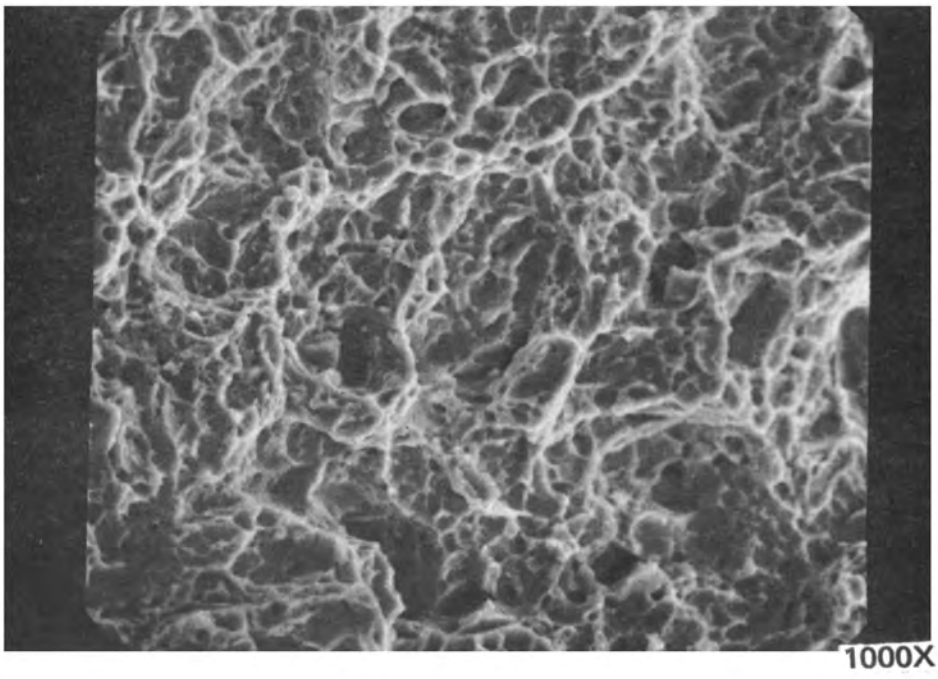

FIGURE 16

PHOTOGRAPHS OF VACUUM CADMIUM FRACTURE AREA

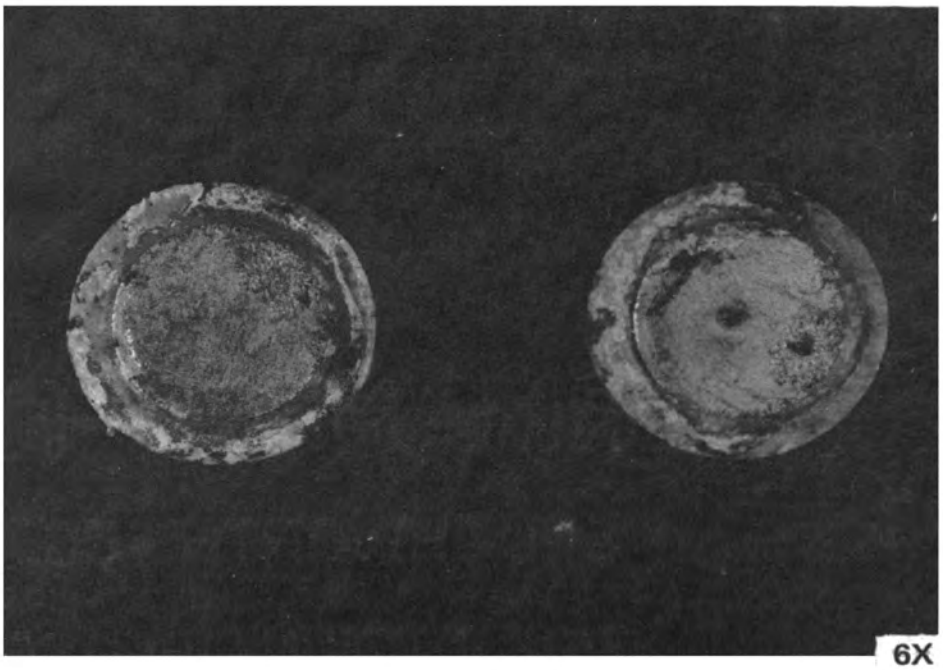

FIGURE 17

MACROPHOTOGRAPHS OF VACUUM CADMIUM (EXPOSED) FRACTURE SURFACES

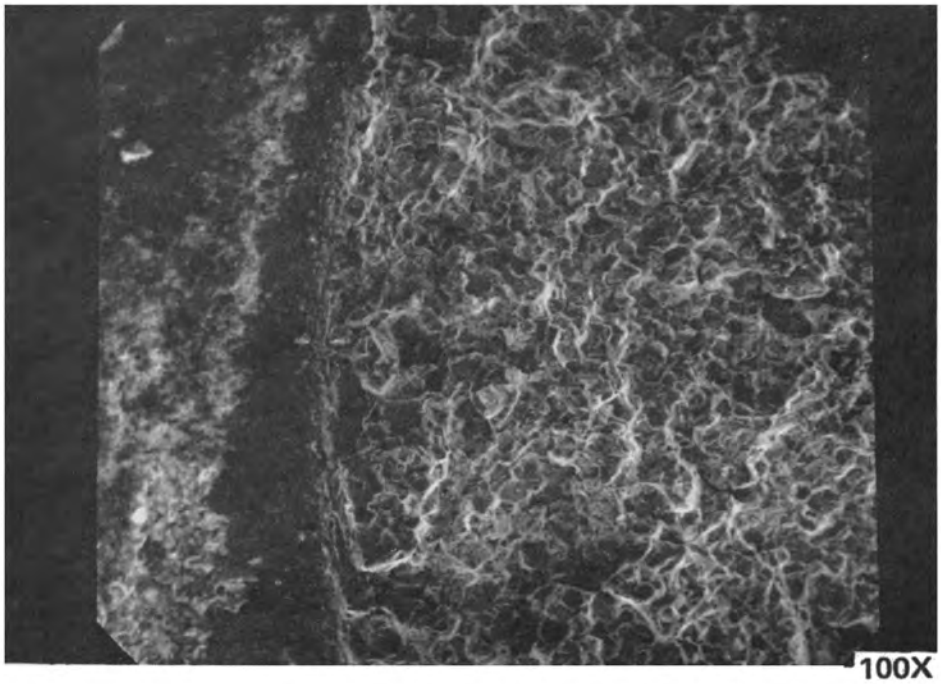

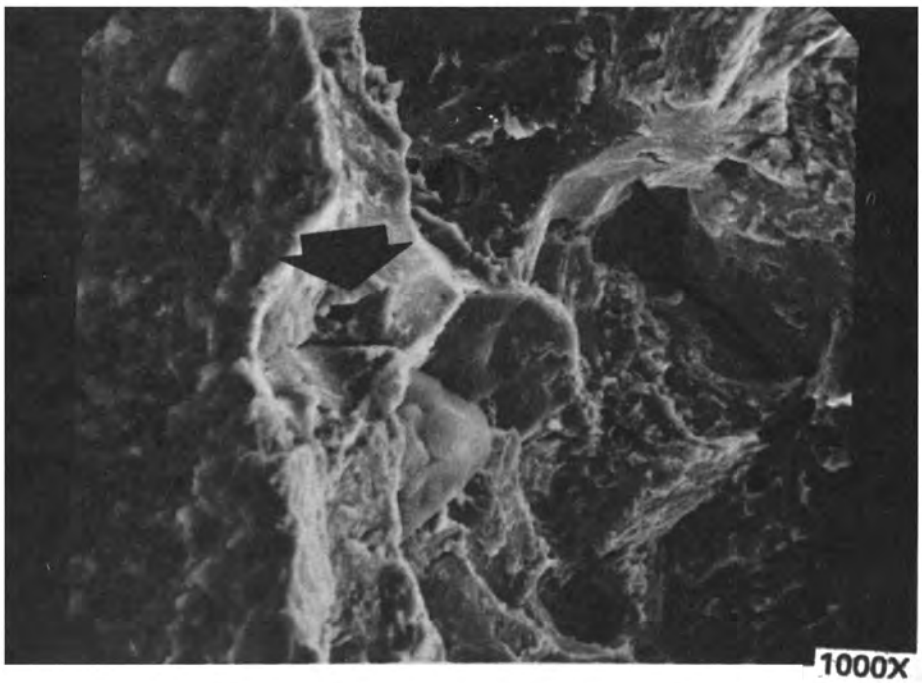

FIGURE 18

PHOTOGRAPHS OF VACUUM CADMIUM (EXPOSED) FRACTURE INITIATION

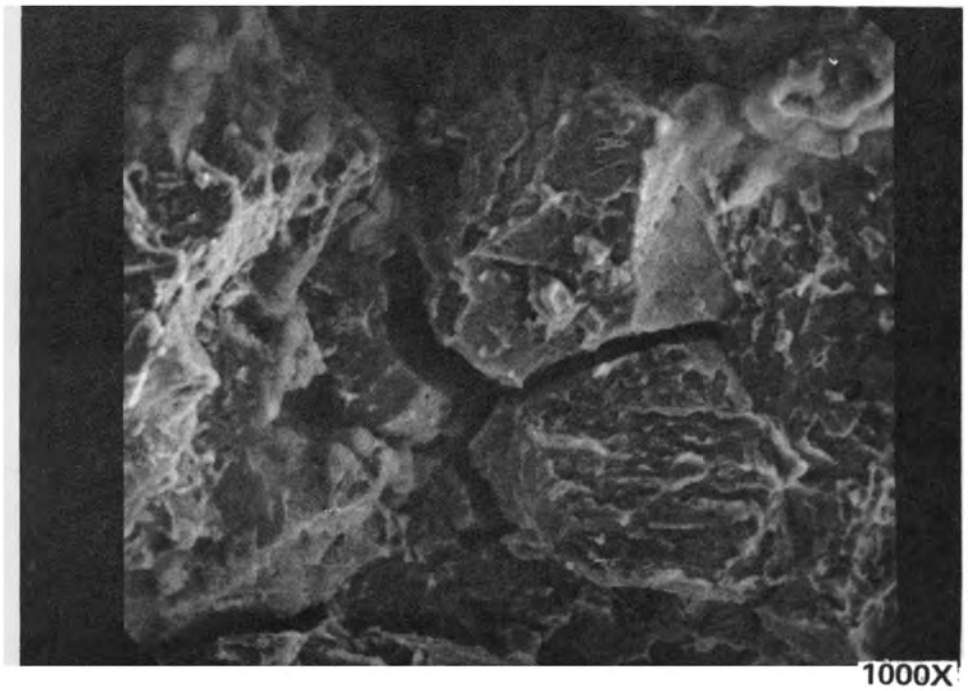

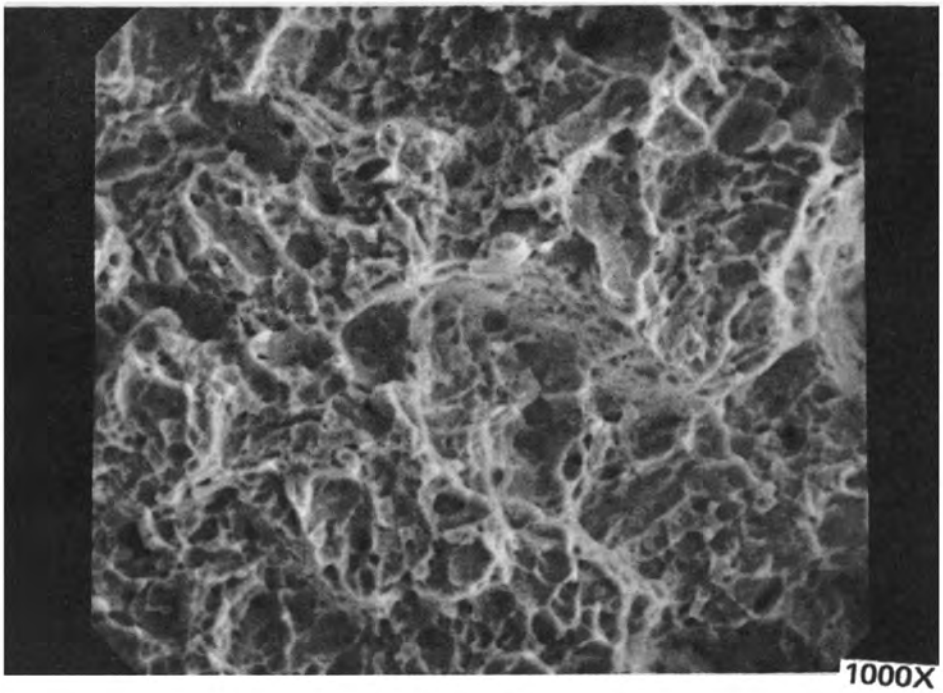

FIGURE 19

PHOTOGRAPHS OF VACUUM CADMIUM (EXPOSED) FRACTURE AREA

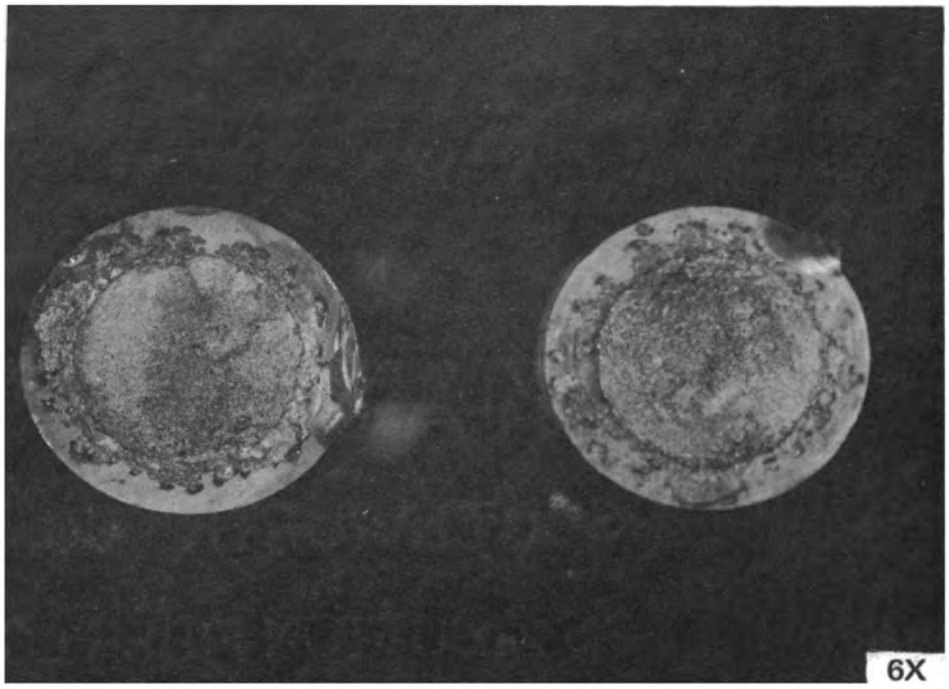

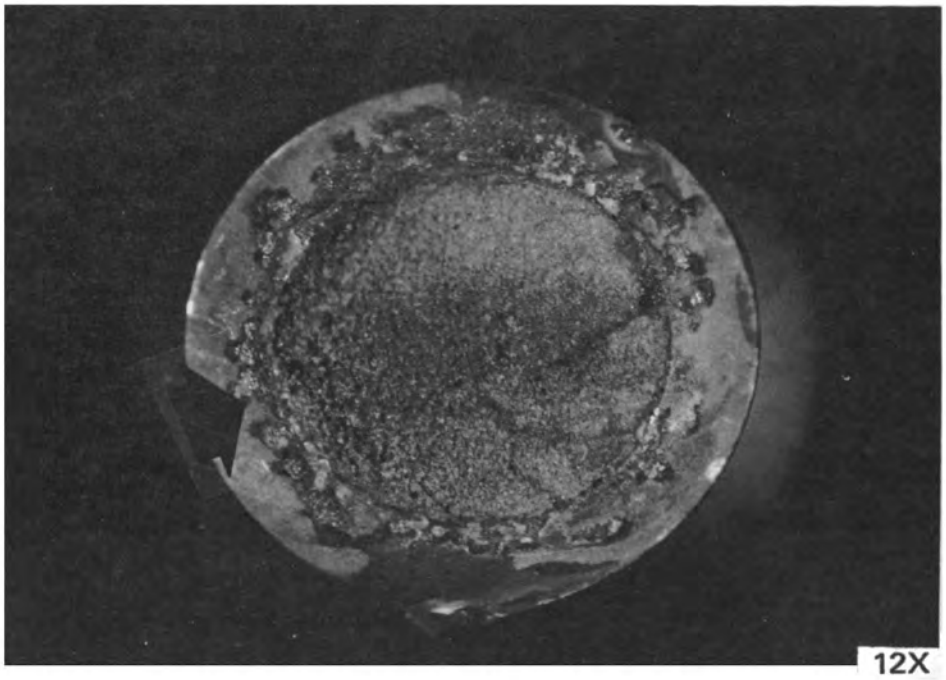

FIGURE 20

MACROPHOTOGRAPHS OF ELECTROPLATE CADMIUM FRACTURE SURFACES

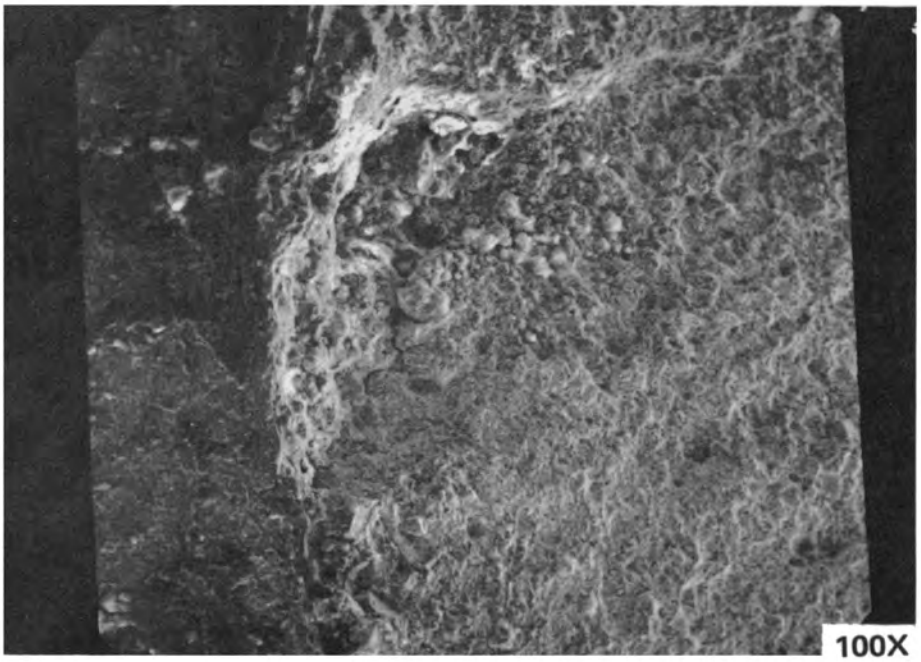

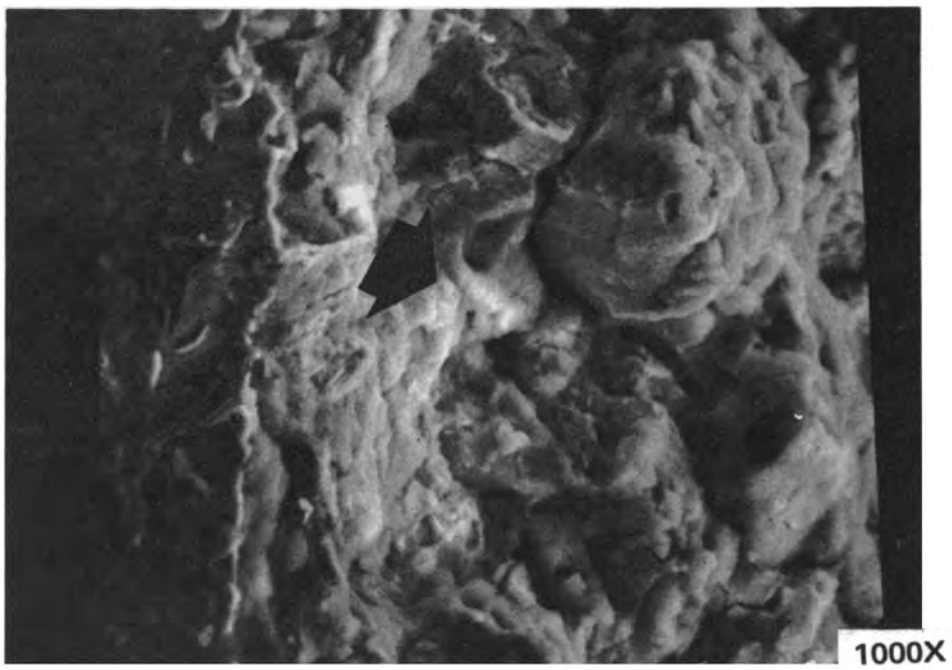

FIGURE 21

PHOTOGRAPHS OF ELECTROPLATE CADMIUM FRACTURE INITIATION

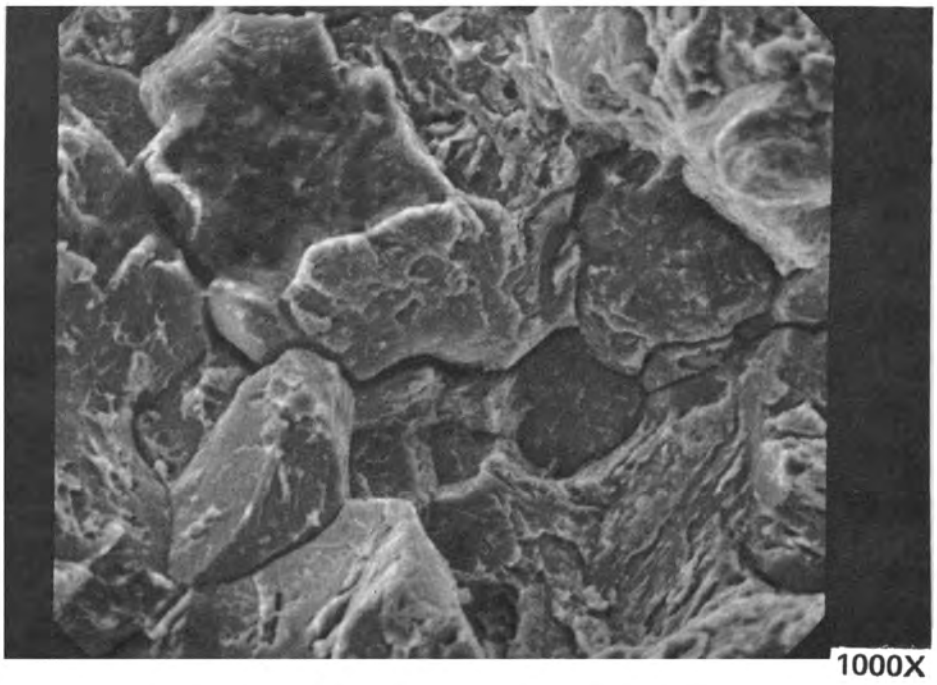

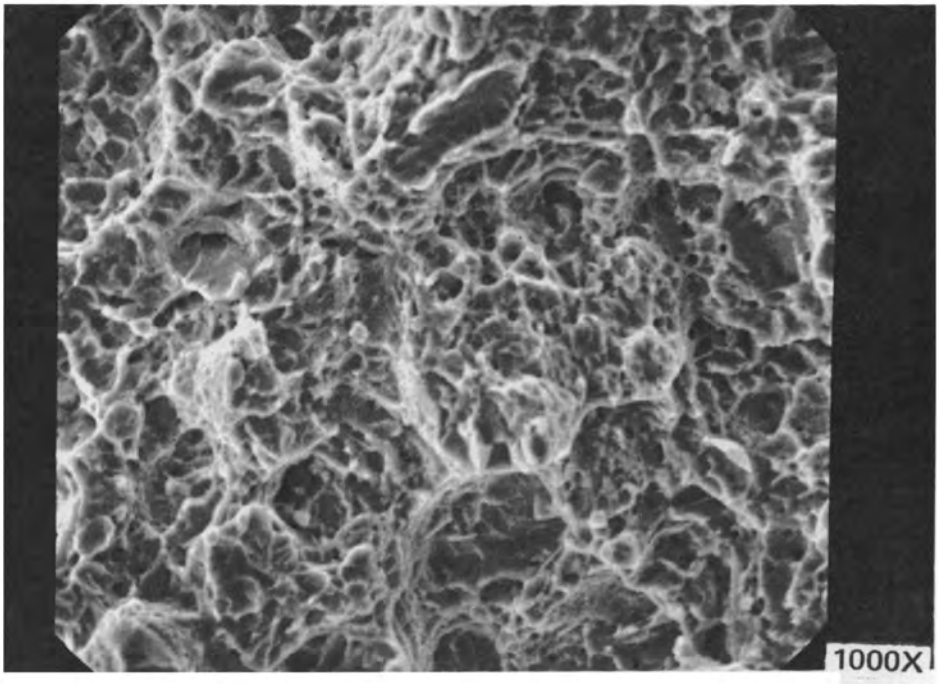

FIGURE 22

PHOTOGRAPHS OF ELECTROPLATE CADMIUM FRACTURE AREA

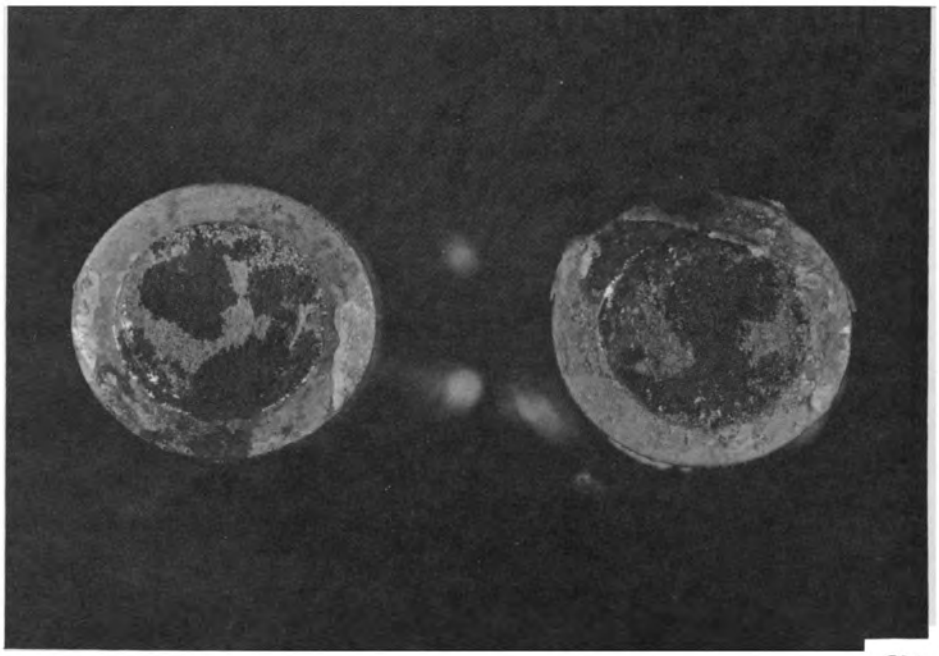

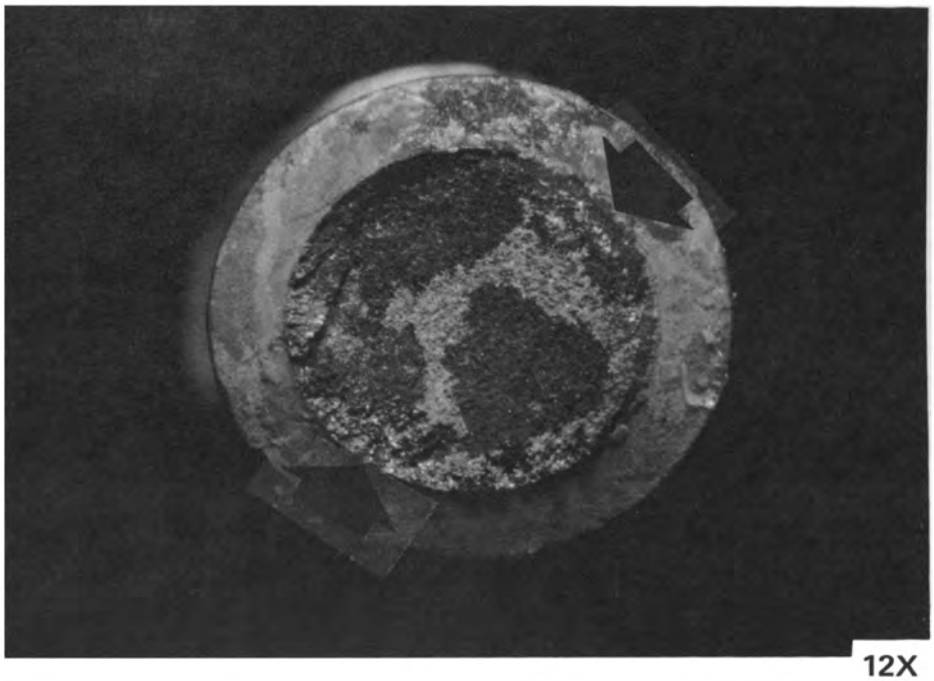

FIGURE 23

MACROPHOTOGRAPHS OF ELECTROPLATE CADMIUM (EXPOSED)

FRACTURE SURFACES

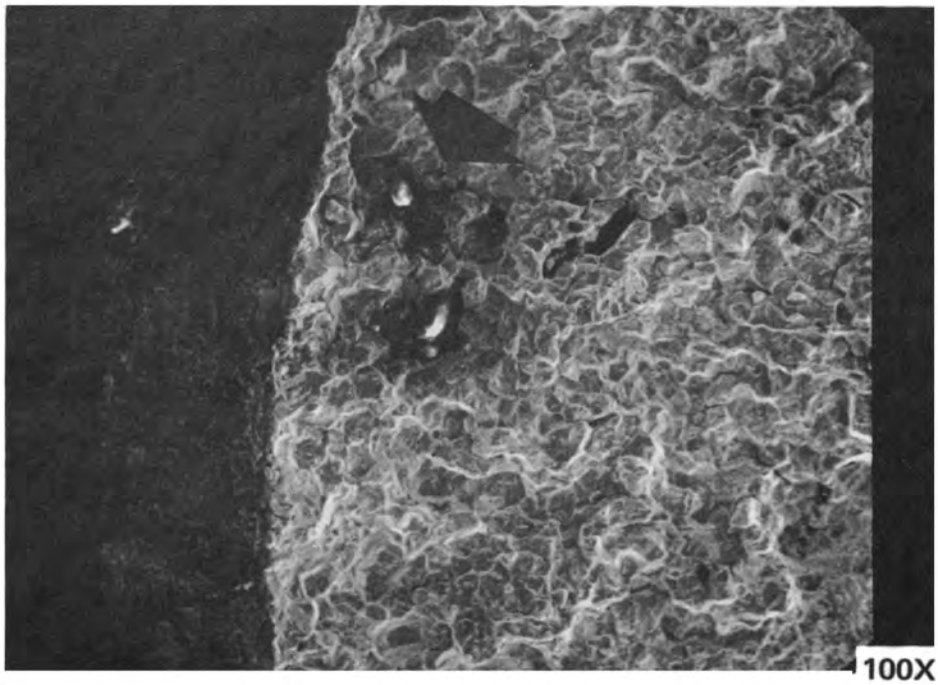

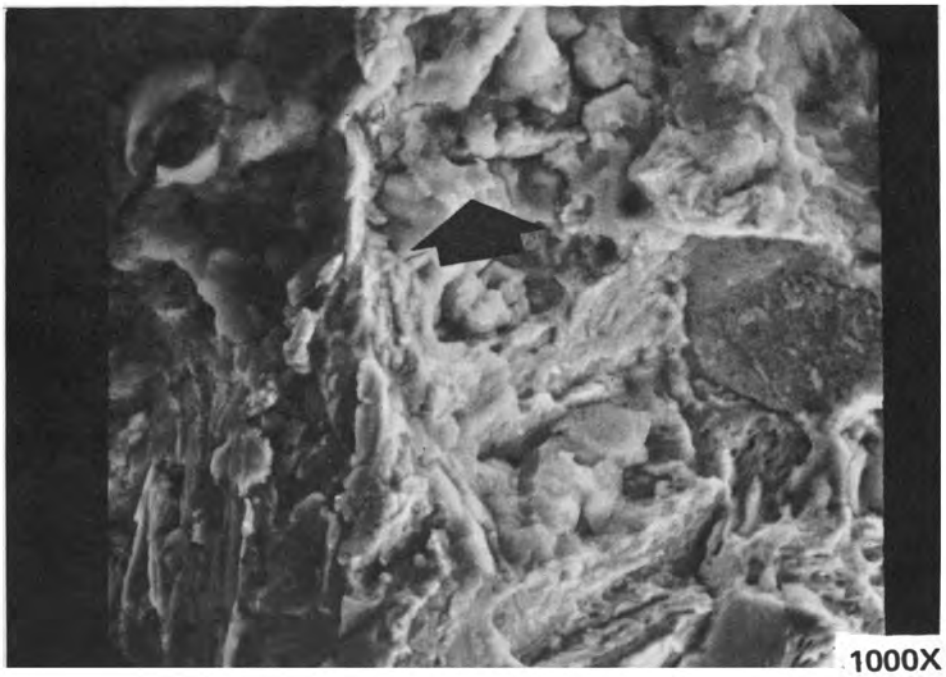

FIGURE 24

PHOTOGRAPHS OF ELECTROPLATE CADMIUM (EXPOSED)

FRACTURE INITIATION

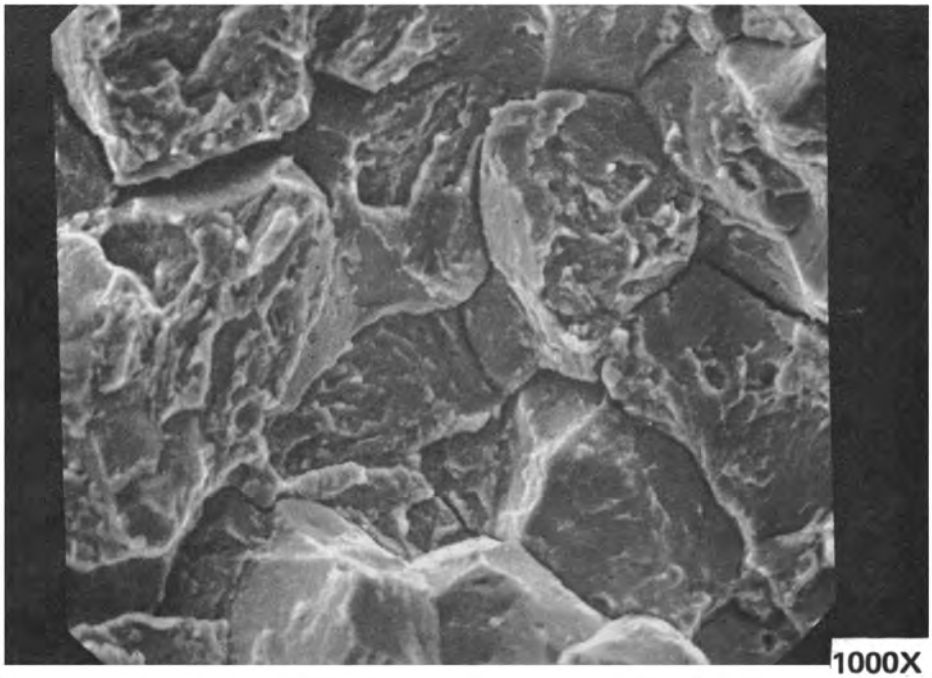

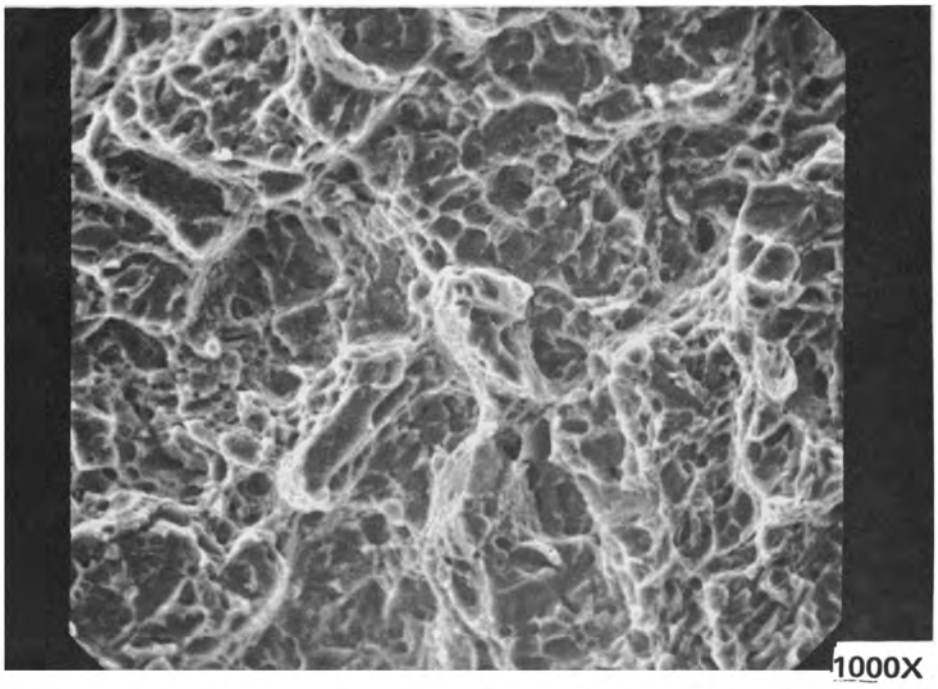

FIGURE 25

PHOTOGRAPHS OF ELECTROPLATE CADMIUM (EXPOSED)

FRACTURE AREA

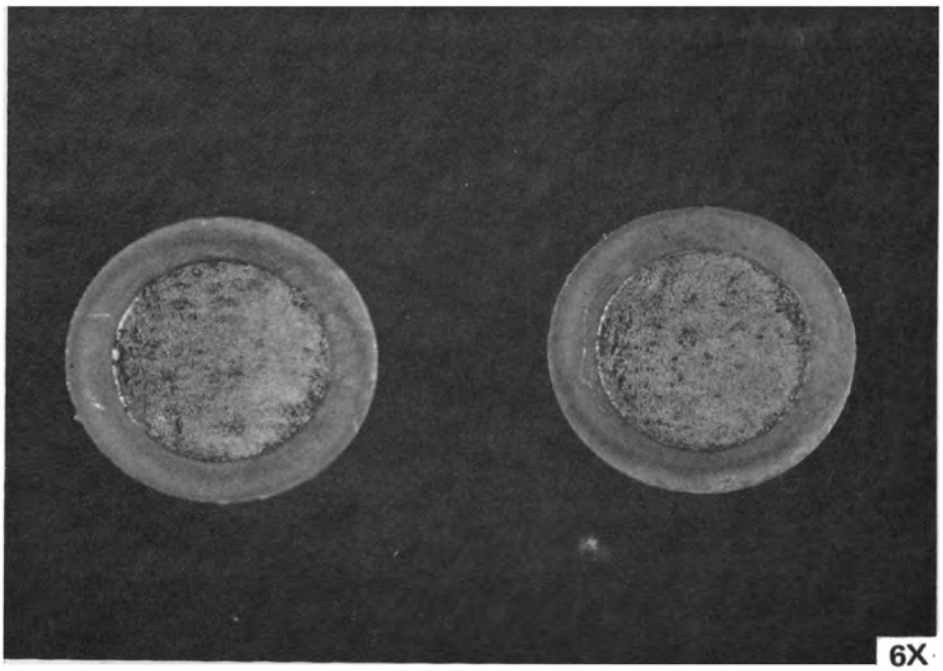

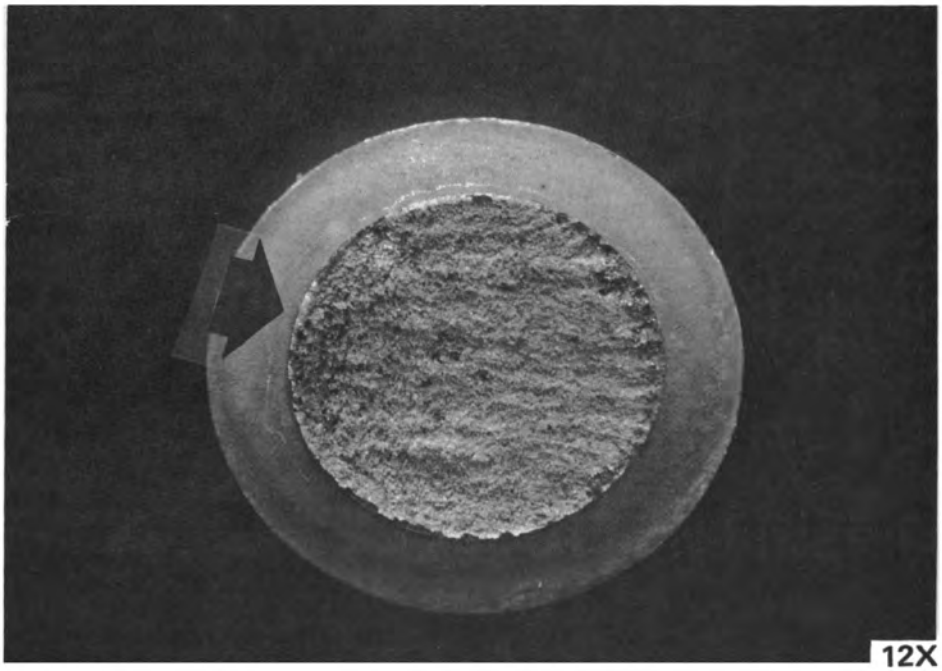

FIGURE 26

MACROPHOTOGRAPHS OF VACUUM ALUMINUM FRACTURE SURFACES

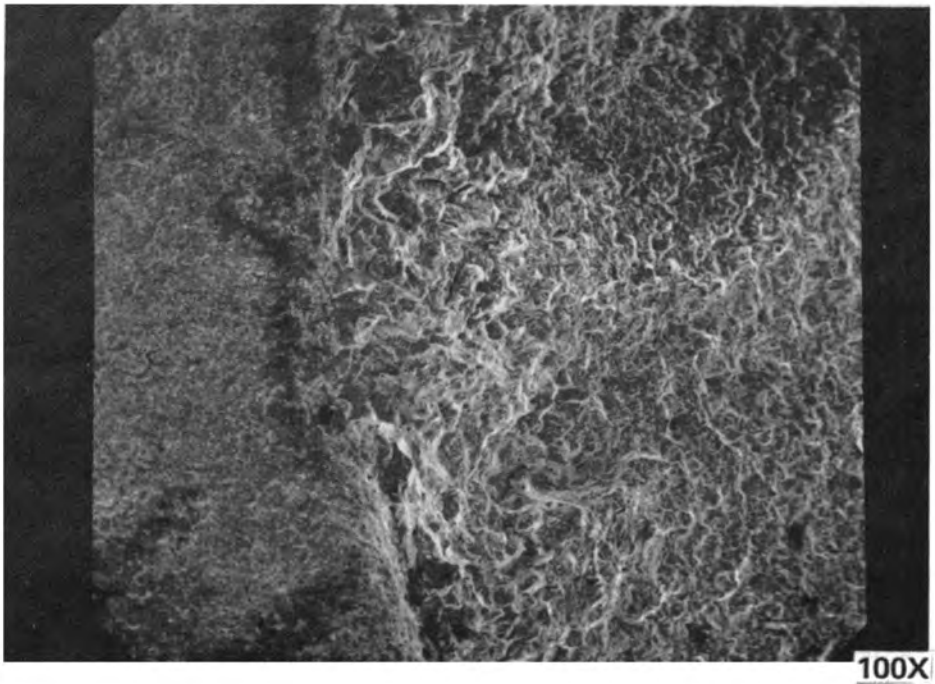

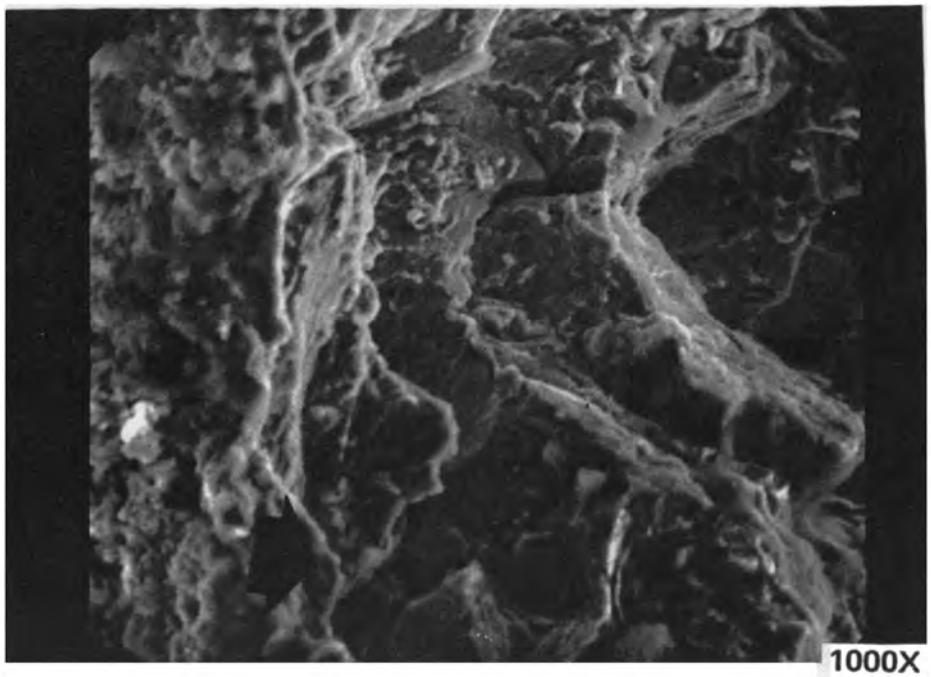

FIGURE 27

PHOTOGRAPHS OF VACUUM ALUMINUM FRACTURE INITIATION

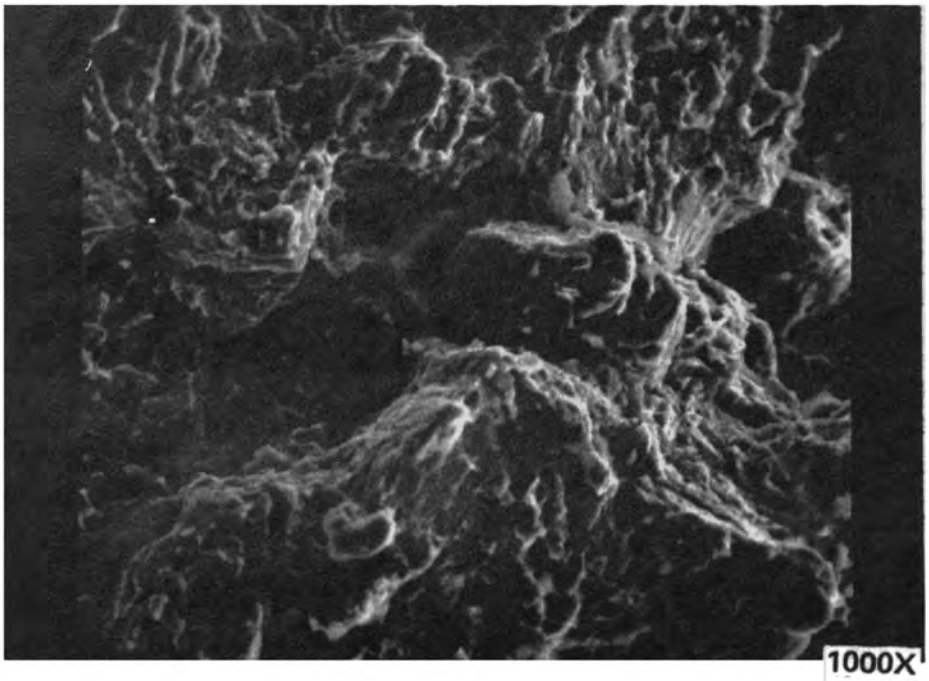

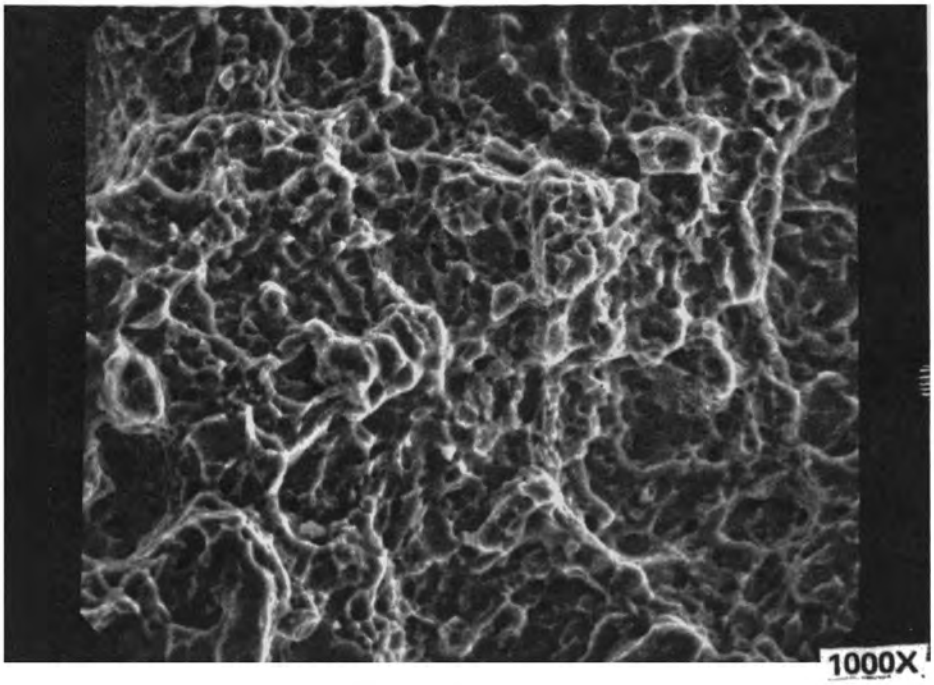

FIGURE 28

PHOTOGRAPHS OF VACUUM ALUMINUM FRACTURE AREA

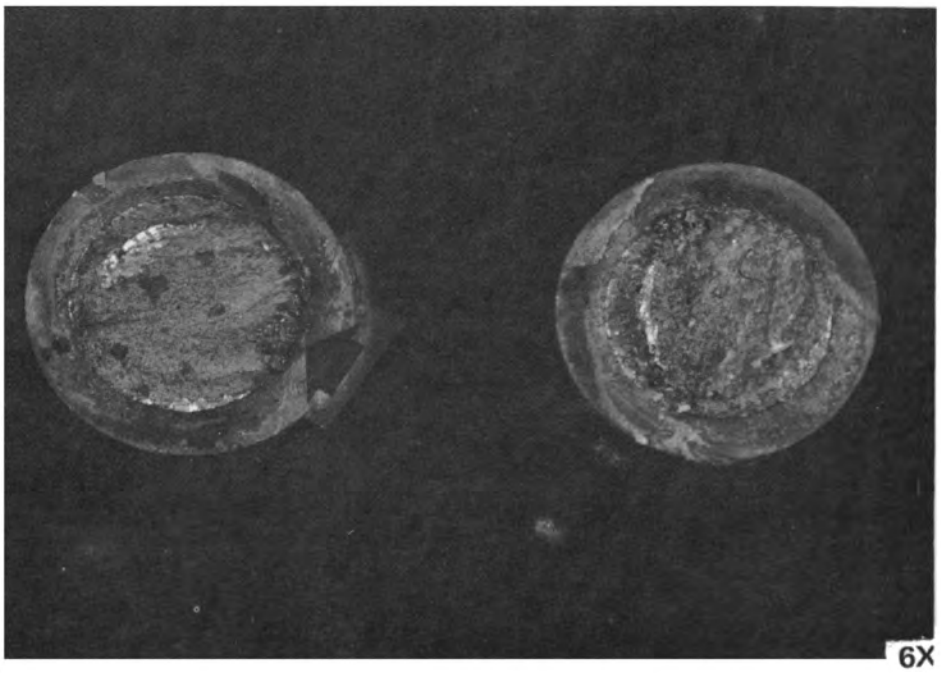

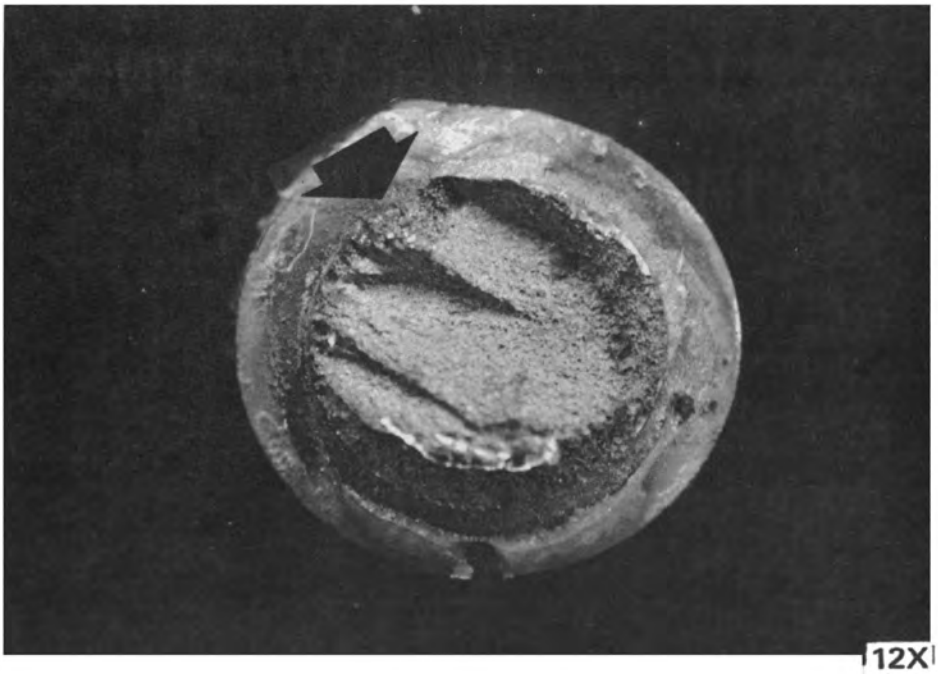

FIGURE 29

MACROPHOTOGRAPHS OF VACUUM ALUMINUM (EXPOSED)

FRACTURE SURFACES

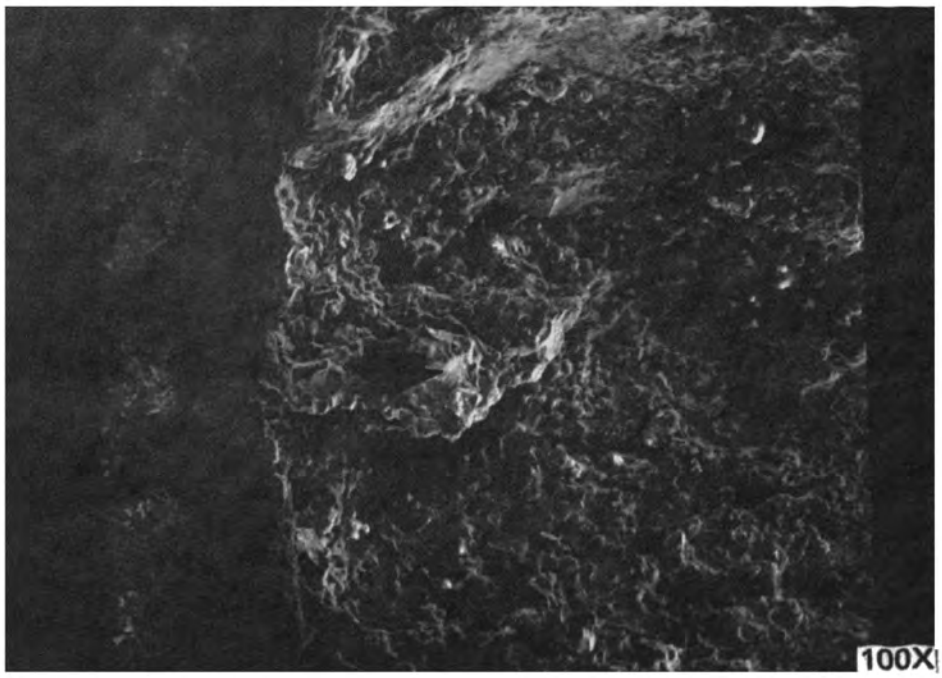

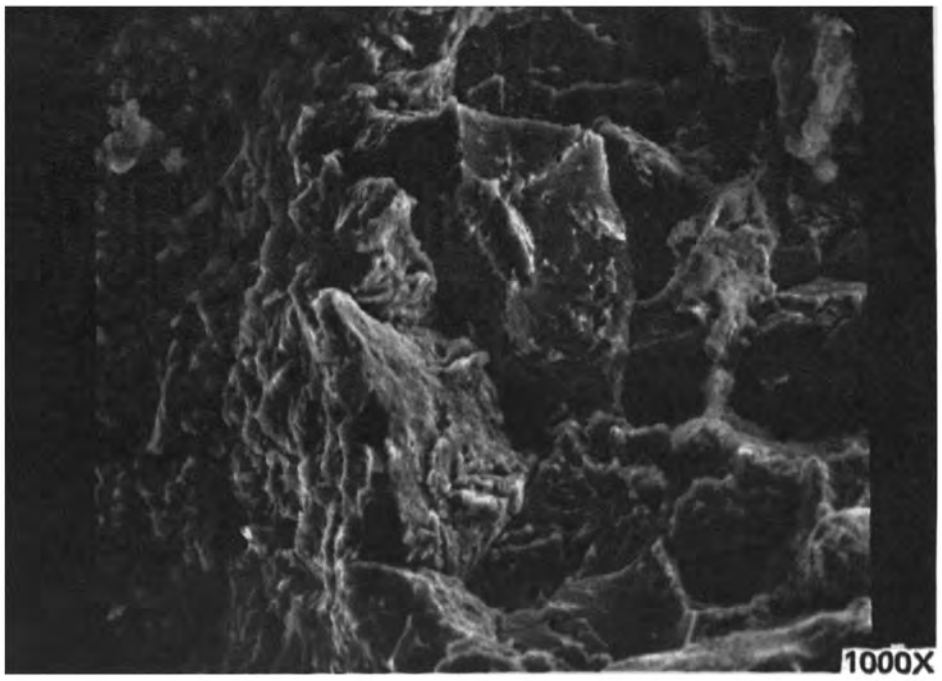

FIGURE 30

PHOTOGRAPHS OF VACUUM ALUMINUM (EXPOSED) FRACTURE INITIATION

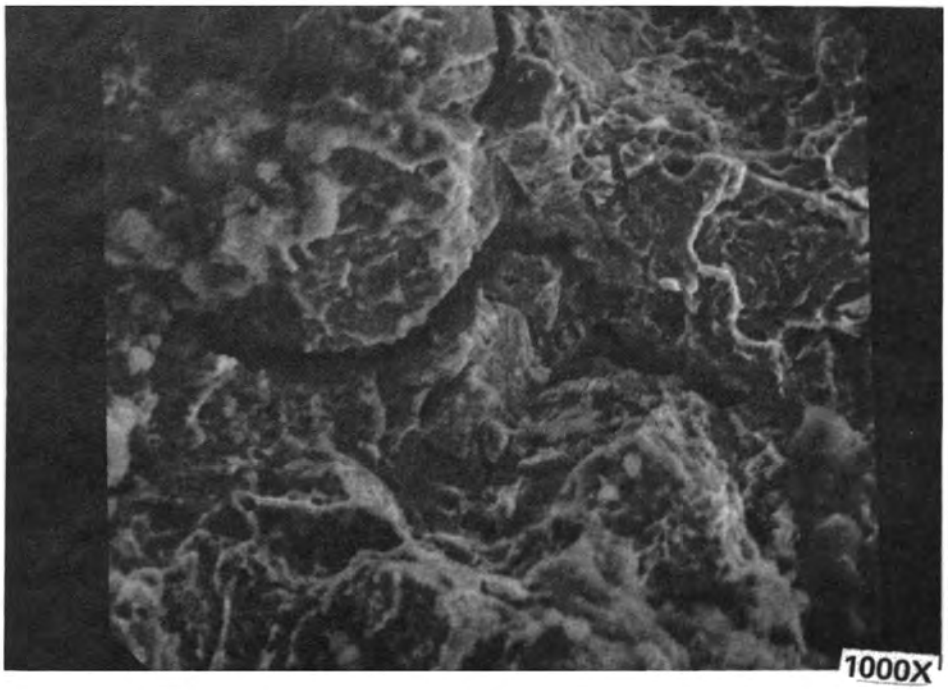

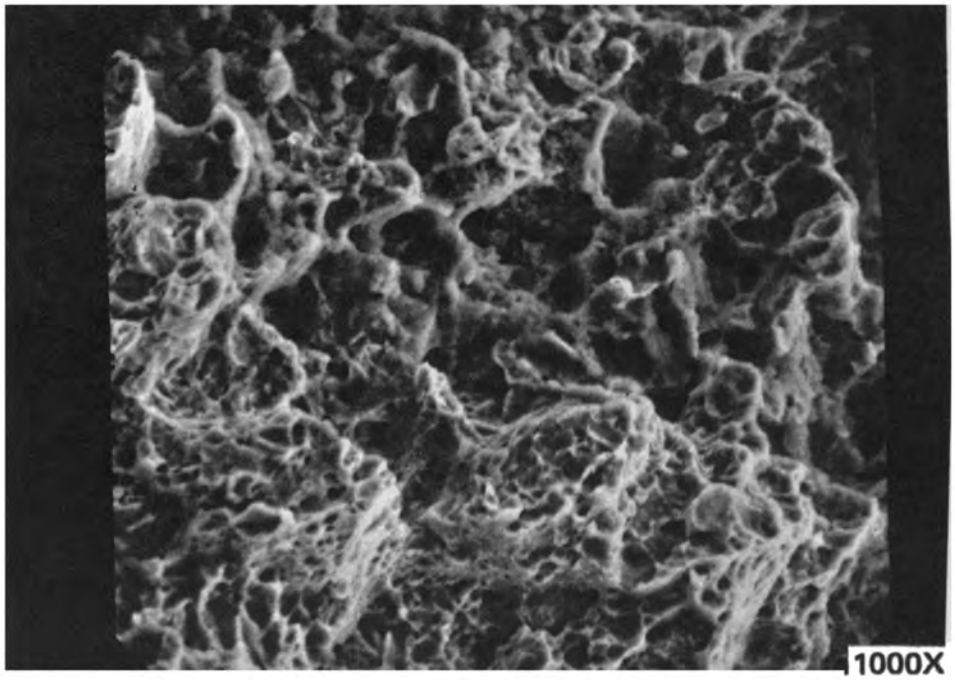

FIGURE 31

PHOTOGRAPHS OF VACUUM ALUMINUM (EXPOSED) FRACTURE AREA

VI. DISCUSSION

It is quite evident from the preceding discussion of the test results that vacuum aluminum and cadmium reduce the stress corrosion resistance of 300M steel when compared with the bare control and the electroplated cadmium. The control specimens were not subjected to cathodic protection; therefore, there was no hydrogen induced into the steel and the failures were purely of a stress corrosion nature. Hydrogen embrittlement resulting from cathodic protection definitely accelerated the failure of the specimens coated with vacuum aluminum and vacuum cadmium. Aluminum and cadmium have half-cell potentials of -1.66 and -0.403 volts, respectively. This indicates that hydrogen is being generated at the steel by the following reaction ($H^+ + e^- \longrightarrow H^\circ$). The half-cell potential for aluminum is larger than the half-cell potential for cadmium. This indicates that the potential for hydrogen to be produced is greater with aluminum and explains why the aluminum coated specimens failed prior to the vacuum cadmium specimens.

It would be reasonable to assume that both vacuum deposited and electroplated cadmium would offer similar cathodic protection characteristics. But, this is not the case, as seen, when Figures 6 and 7 are compared. To explain the difference, an additional picture was taken with the

scanning electron microscope. Figure 32 is a comparison of the physical surface of both types of coatings. The vacuum cadmium coating is granular and appears porous, while the electroplated cadmium is smooth and continuous. The electroplated cadmium presents a good barrier to prevent diffusion of the hydrogen into the base steel. Vacuum aluminum is also porous like vacuum cadmium and allows easy diffusion of hydrogen to the base steel.

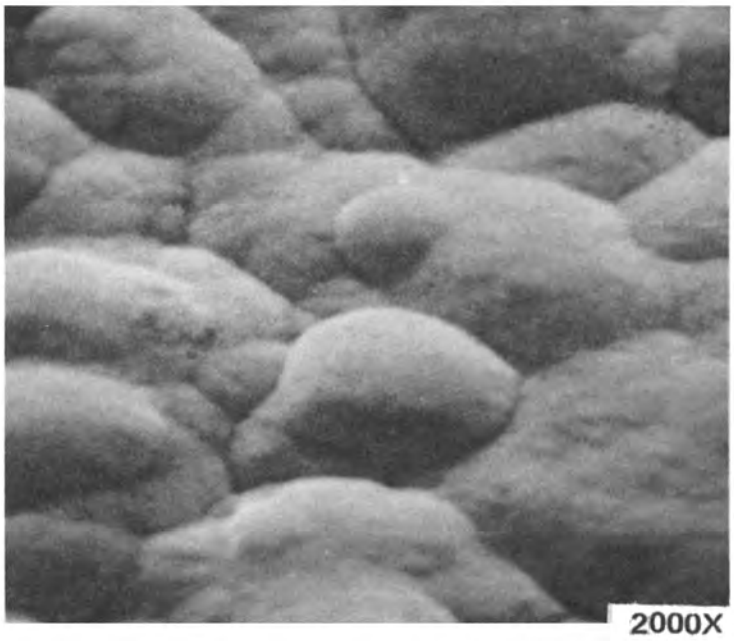

ELECTROPLATED CADMIUM

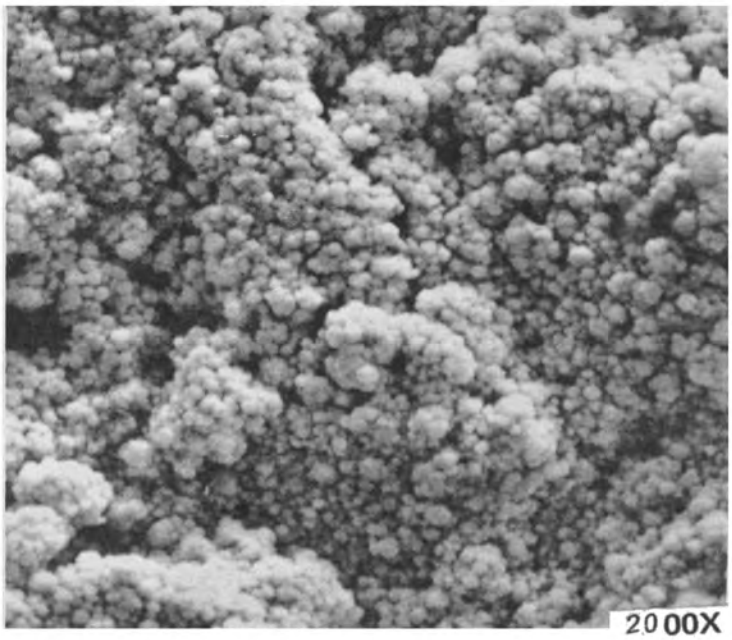

VACUUM CADMIUM

FIGURE 32

SURFACE PHOTOGRAPHS OF VACUUM AND ELECTROPLATED CADMIUM

VII. CONCLUSIONS

The results of this thesis program indicate the following for 300M low alloy steel:

1) Hydrogen produced during cathodic protection of 300M steel by vacuum aluminum and vacuum cadmium causes hydrogen embrittlement and accelerates the stress corrosion failure.

2) Cathodic protection afforded by vacuum cadmium accelerates stress corrosion of 300M steel at all stress levels and significantly below 60% NTS. The failure mechanism is most pronounced below 60% NTS because time is needed for the hydrogen to diffuse through the dense cadmium coating.

3) Vacuum aluminum does not afford adequate cathodic protection to 300M steel and failure can be expected at all stress levels.

4) Electroplated cadmium affords excellent cathodic protection to 300M steel because it acts as a barrier against hydrogen entry and corrosion process.

5) A notch through the cathodic coating to the base steel does not increase the failure susceptibility of 300M steel. The large anode to cathode ratio protects the steel from corroding and the hydrogen produced is not concentrated on the steel.

BIBLIOGRAPHY

1. BERRY, W. E., E. E. FLETCHER, and A. R. ELSEA (1966) - Stress corrosion cracking and hydrogen stress cracking of high strength steel. DMIC Report 232, Battelle Memorial Institute, Columbus, Ohio, p. 1-5.

2. COPSON, H. R. (1954) - Laboratory techniques for the investigation of stress corrosion cracking. Electrochemical Society Symposium on Stress Corrosion Cracking and Embrittlement, Boston, Mass., p. 187-190.

3. ELSEA, A. R. and E. E. FLETCHER (1965) - Hydrogen movement in steel--entry, diffusion, and elimination. DMIC Report 219, Battelle Memorial Institute, Columbus, Ohio, p. 20-24.

4. HANNA, G. L., A. R. TROIANO, and E. A. STEIGERWALD (1964) - A mechanism for the embrittlement of high-strength steels by aqueous environments. Transactions of the ASM, 57, p. 658-659.

5. YAMAOKA, H. and G. WRANGLEN (1966) - An electrochemical study of the cracking of stressed high-strength low alloy martensitic steels in water. Corrosion Science, 6, p. 113-116.

6. HILDEBRAND, J. F., E. W. TURNS, and F. C. NORDQUIST (1967) - Stress corrosion cracking in high strength ferrous alloys. U.S. Department of Commerce, AD-423 387, p. 14-20.

7. STEIGERWALD, E. A. and G. L. HANNA (1962) - Initiation of slow crack propagation in high-strength materials. Proceedings of Sixty-fifth Annual Meeting of the ASTM, 62, p. 885- 889.

8. HILL, M. L. (1960) - The behavior of hydrogen in iron and steel. Proceedings of the 47th American Electroplaters Society, Los Angeles, California, p. 124.

9. TROIANO, A. R. (1959) - Delayed failure of high strength steels. Corrosion, 15, p.207.

10. JOHNSON, H. H., J. G. MORLET, and A. R. TROIANO (1958) - Hydrogen, crack initiation, and delayed failure of steel. Transactions of AIME, 1958, p. 528.

11. ZAPFFE, C. and C. E. SIMS (1940) - Defects in welded metals and hydrogen in steel. Welding Journal, 19, p. 377-385.

12. ZAPFFE, C. and C. E. SIMS (1941) - Hydrogen embrittlement, internal stress and defects in steel. Transactions of AIME, 145, p.225-230.

13. MORLET, J. G., H. H. JOHNSON, and A. R. TROIANO (1958) - A new concept of hydrogen embrittlement in steel. Journal of Iron and Steel Institute, 149, p. 37-44.

14. DIX, E. H. (1940) - Acceleration of the rate of corrosion by high constant stresses. Transactions of AIME, 137, p. 16-21.

15. KEATING, F. H. (1948) - Stress corrosion mechanisms in high strength steels. Symposium on Internal Stresses in Metals and Alloys, Institute of Metals, p. 311.

16. MEARS, R. B., R. H. BROWN, and E. H. DIX (1945) - Symposium of Stress Corrosion Cracking of Metals, ASM- AIME Joint Symposium, Philadelphia, Pa. p. 323.

17. GILBERT, P. T. and S. E. HADDEN (1950) - A theory of the mechanism of stress corrosion in aluminum-7% magnesium alloys. Journal Institute of Metals, 77, p. 237.

18. DEEGAN, D., I. MATSUSHIMA, and H. H. UHLIG (1961) - Stress corrosion and hydrogen cracking of 17-7 stainless steel. Corrosion 22, p. 23.

19. ELSEA, A. R. and MCEOWEN L. J. (1965) - Behavior of high strength steels under cathodic protection. Corrosion, 21, p. 28-31.

20. ELSEA, A. R. (1970) - A personal conversation with the author April 20, 1970. Thesis laboratory notebook.

21. BARNARTT, S. (1962) - General concepts of stress-corrosion cracking. Corrosion 18, p. 21.

22. SONNINO, C. B. (1969) - Experimental research on stress corrosion behavior of maraging steels in various environments. Revue de Metallurgie, November 1969, p. 742-744.

23. HYTER, W. (1970) - A personal conversation with the developer of the test method for Douglas Aircraft, May 3, 1970. Thesis laboratory notebook.

24. FANNIN, E. R. (1970) - A personal conversation with the author to determine advantages of the test method, May 10, 1970. Thesis laboratory notebook.

25. NATHORST, N. (1950) - Stress corrosion of stainless steels. Welding Research Council Bulletin Series, No. 6, October, p. 3-6.

26. LIN, C. S., J. J. LAURILLIARD and A. C. HOOD (1967) - Stress corrosion cracking of high strength bolting. Stress Corrosion Testing, ASTM STP 425, Am. Soc. Testing Materials, p. 84.

27. GEYER N. M., G. W. LAWLESS and B. COHEN (1960) - A new look at the hydrogen embrittlement of cadmium coated high strength steels. Proceedings of the 47th American Electroplaters Society, Los Angles, California p.143-145.

28. KETCHAM, S. J. and SUBCOMMITTEE MEMBERS (1966) - Stress corrosion testing methods. Stress Corrosion Testing, ASTM STP 425, Am. Soc. Testing Materials, p. 3.

29. KERLINS V., A. PHILLIPS, R. A. RAWE and B. V. WHITESON (1968) - Electron fractography handbook specific applications of electron fractography. Technical Report AFML-TR-64-416, United States Air Force, p. (5-1) - (5-4).

APPENDIX 1

TEST SPECIMEN DIMENSIONS

Specimen Number	Notch Diameter (inch)	Notch Root Radius (inch)
1	0.1765	---
2	0.1770	---
3	0.1773	---
4	0.1774	0.0025
5	0.1753	0.0028
6	0.1748	0.0035
7	0.1761	0.0032
8	0.1720	0.0030
9	0.1730	0.0033
10	0.1750	0.0028
11	0.1755	0.0030
12	0.1750	0.0028
13	0.1744	0.0034
14	0.1750	0.0032
15	0.1790	0.0032
16	0.1745	0.0030
17	0.1730	0.0030
18	0.1750	0.0035
19	0.1785	0.0028
20	0.1773	0.0030
21	0.1750	0.0031
22	0.1750	0.0028
23	0.1743	0.0030
24	0.1764	0.0028
25	0.1755	0.0032
26	0.1744	0.0032
27	0.1755	0.0033
28	0.1748	0.0040
29	0.1750	0.0030
30	0.1750	0.0032
31	0.1761	0.0032
32	0.1750	0.0032
33	0.1751	0.0035
34	0.1750	0.0034
35	0.1767	0.0035
36	0.1752	0.0028
37	0.1750	0.0032
38	0.1745	0.0030
39	0.1755	0.0032
40	0.1753	0.0030
41	0.1750	0.0033
42	0.1750	0.0032
43	0.1760	0.0035
44	0.1754	0.0032
45	0.1746	0.0035
46	0.1755	0.0030

Specimen Number	Notch Diameter (inch)	Notch Root Radius (inch)
47	0.1750	0.0032
48	0.1743	0.0033
49	0.1755	0.0032
50	0.1750	0.0035
51	0.1745	0.0036
52	0.1746	0.0034
53	0.1770	0.0032
54	0.1763	0.0030
55	0.1745	0.0033
56	0.1786	0.0032
57	0.1747	0.0032
58	0.1755	0.0032
59	0.1750	0.0028
60	0.1778	0.0034
61	0.1747	0.0030
62	0.1746	0.0032
63	0.1747	0.0046
64	0.1750	0.0030
65	0.1756	0.0037
66	0.1749	0.0032
67	0.1730	0.0027
68	0.1755	0.0032
69	0.1746	0.0033
70	0.1752	0.0035
71	0.1750	0.0035
72	0.1750	0.0032
73	0.1767	0.0030
74	0.1761	0.0034
75	0.1770	0.0028
76	0.1774	0.0032
77	0.1750	0.0032
78	0.1750	0.0035
79	0.1745	0.0032
80	0.1765	0.0031
81	0.1757	0.0034
82	0.1753	0.0029
83	0.1749	0.0028
84	0.1750	0.0032
85	0.1745	0.0034
86	0.1745	0.0032
87	0.1750	0.0035
88	0.1750	0.0032
89	0.1753	0.0033
90	0.1740	0.0035
91	0.1703	0.0034
92	0.1765	0.0034
93	0.1751	0.0032

APPENDIX 2

TEST SPECIMEN LOADING DATA

Load (#)	Average Strain (Strain 1 - Strain 2)/2 (μ-inch/inch)	Notch Tensile Stress (KSI)	Test Load (% NTS)
200	175	9	
400	330	17	
600	510	26	
800	650	34	
1000	800	43	
1200	940	51	
1400	1080	60	
1600	1325	69	
1800	1470	79	
2000	1610	86	
2200	1750	94	
2400	1890	103	
2600	2030	111	
2800	2165	120	
3000	2310	129	
3200	2440	137	
3400	2585	146	
3600	2725	154	
3800	2955	163	41
4000	3005	172	
4200	3150	180	
4400	3325	189	
4600	2424	197	
4800	3680	206	
5000	3720	214	
5200	3870	223	
5700	4225	244	61
6000	4440	258	
6500	4205	279	
7000	4510	300	75
7500	4930	322	
8000	5300	343	
8500	5655	365	91
9000	6030	386	
9300	6410	399	

VITA

John Pechonick was born October 3, 1943 in Loretto, Tennessee. He received his primary and secondary education at West Jackson and Jackson High School in Jackson, Tennessee. At the University of Missouri - Rolla in January 1966, the author was awarded a Bachelor of Science Degree in Chemical Engineering.

He has been enrolled in the St. Louis Graduate Extension Center of the University of Missouri - Rolla since January 1968. He has been employed at McDonnell-Douglas Aircraft Corporation, St. Louis, Missouri, since January 1966.